Article

Dscamb regulates cone mosaic formation in zebrafish via filopodium-mediated homotypic recognition

Dongpeng Hu ⓘ & Ichiro Masai ⓘ ✉

Cone photoreceptors assemble to form a regular mosaic pattern in vertebrate retinas. In zebrafish, four distinct spectral cone types (red, green, blue, and ultraviolet), form a lattice-like pattern. However, the mechanism of cone mosaic formation has been unknown. Here we show that Down Syndrome Cell Adhesion Molecule b (Dscamb) regulates the cone mosaic pattern in zebrafish, especially via red-cone spacing. During photoreceptor differentiation, newly formed cones extend filopodium-like processes laterally to apical surfaces of neighboring cones. Interestingly, red cones extend filopodia, but promptly retract them when they meet their own cone type, suggesting filopodium-mediated, homotypic recognition and self-avoidance. This self-avoidance is compromised in zebrafish *dscamb* mutants, leading to abnormal clustering of red cones and subsequent disruption of regular cone spacing. Thus, apical filopodium-mediated spacing of the same cone type depends on Dscamb and is essential for cone mosaic formation in zebrafish.

Cone photoreceptors assemble to form a regular mosaic pattern in vertebrates[1]. In zebrafish adult retinas, four types of cones with different peak absorbances at red, green, blue, and ultra-violet (UV) wavelengths[2], form a lattice-like pattern, in which rows of red and green double-cone pairs alternate with rows of blue and UV single cones[3,4] (Fig. 1a). Furthermore, three types of cones, red, green, and blue, are tightly associated via apical polarity regulators, Crumbs2b (Crb2b) and Ponli, at the inner segment region of photoreceptors, to form a pentameric cone unit (green-red-blue-red-green)[5,6]. However, the most central region of adult zebrafish retinas, which is of embryonic origin, does not show the precise lattice-like pattern, although each cone type displays regular spacing[7] (Fig. 1b).

During zebrafish retinal development, a regulatory network of transcription factors controls fate determination of different retinal cell-types from equipotent retinal progenitor cells[8]. In zebrafish, each cone-type is generated by symmetric terminal division of its dedicated cone precursors[9]. Three transcription factors, namely Thyroid hormone receptor beta (Thrb), Foxq2, and Tbx2b, promote differentiation of red, blue, and UV cones, respectively, in zebrafish[9–11]. In addition, Sine oculis homeobox 6 and 7 (Six6 and Six 7) cooperate to promote the differentiation of green and blue cones[12]. The cone mosaic pattern

is disrupted by the loss of both blue and green cones in *six6a/six6b/six7* triple knockout zebrafish[12], as well as by loss of UV cones in *tbx2b* mutants[13]. Crb2b stabilizes the pentameric cone unit[5]. However, cone mosaic formation is normal in *crb2b* mutants, although the pattern degrades in an age-dependent manner[14]. Thus, no molecule that directly regulates the formation of the cone mosaic pattern has been identified.

Down Syndrome Cell Adhesion Molecule (DSCAM) is an immunoglobulin (Ig) superfamily protein, which possess 10 Ig domains and 6 fibronectin type III domains in the extracellular region, conserved across invertebrate and vertebrate species[15]. DSCAM is essential for self-avoidance mechanisms in nervous system development[16,17]. These mechanisms are classified as isoneuronal self-avoidance, which discriminates between self and non-self, and homotypic self-avoidance, which discriminates between the same and different cell-types. The role of DSCAM in isoneuronal self-avoidance was studied in *Drosophila melanogaster*[18]. In *Drosophila*, Dscam1 encodes 19,008 isoforms via mutually exclusive alternative splicing of exons 4, 6, and 9, which correspond to Ig2, Ig3 and Ig7 domains, respectively[15]. Fly Dscam1 shows preferential isoform-specific homophilic binding, specificity of which depends on matching of Ig2, Ig3, and Ig7 variable domains[19].

Developmental Neurobiology Unit, Okinawa Institute of Science and Technology Graduate University, Onna, Okinawa, Japan. ✉e-mail: masai@oist.jp
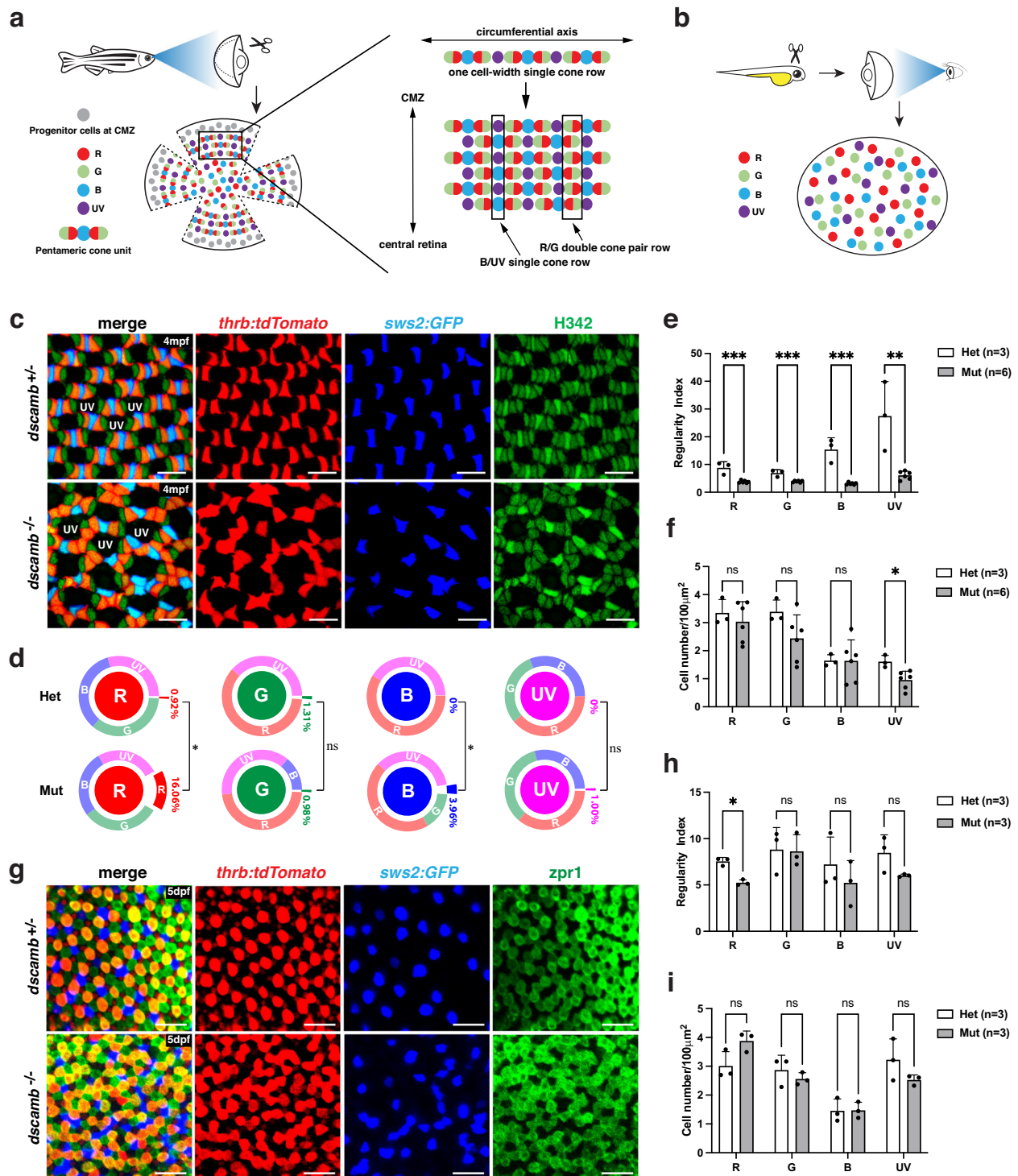
Fig. 1 | Zebrafish *dscamb* mutants show abnormal cone mosaic patterns. a The cone mosaic in zebrafish adult peripheral retinas. Retinal stem cells in the ciliary marginal zone (CMZ) continuously generate cones. Red, green, and blue cones form pentameric cone units. In the circumferential axis, a one-cell-width single-cone row, in which UV cones alternate with pentameric cone units, is formed. This circumferential single-cone row is repeatedly aligned to form the lattice-like cone mosaic, in which red/green double-cone pair rows and UV/blue single-cone rows appear alternately along the periphero-central axis. **b** Zebrafish embryonic cone mosaic. The embryonic cone mosaic is less regular; however, each cone type shows relatively equal spacing. **c** The cone mosaic pattern of 4 mpf *Tg[thrb:tdTomato; sws2:GFP]* transgenic peripheral retinas, which visualize red cones (red) and blue cones (blue), respectively. All cone nuclei were counter-stained with Hoechst33342 (green). The nuclei of UV cones are not visible in this confocal plane. Three independent experiments. **d** The percentage of homotypic and heterotypic contacts for each cone type in adult peripheral retinas. Comparisons between *dscamb* mutants (n = 6) and heterozygous siblings (n = 3) were performed using unpaired two-tailed t-tests. *p < 0.05. **e, f** Regularity index **e** and cell density **f** for each cone type in adult peripheral retinas of heterozygous siblings (n = 3) and *dscamb* mutants (n = 6). **g** ONL in 5 dpf *Tg[thrb:tdTomato; sws2:GFP]* transgenic retinas labeled with zpr1 antibody that visualizes double-cone-type photoreceptors (red/green cones). Three independent experiments. **h** Regularity index of each cone type in embryonic retinas of heterozygous siblings (n = 3) and *dscamb* mutants (n = 3). **i** Density of each cone type in embryonic retinas of heterozygous siblings (n = 3) and *dscamb* mutants (n = 3). Scale bars: 10 μm **c, g. e, f, h, i** Mean ± SD. Statistical significance was evaluated with an unpaired t-test (two tailed): *p < 0.05, **p < 0.01, ***p < 0.001, ns: not significant. **d–f, h, i** Source data and p-values are provided as Source Data for Fig. 1.

Importantly, each neuron stochastically produces different subsets of Dscam1 isoforms, which confer a cell identity code for isoneuronal self-recognition[20–22]. Dscam1 also regulates axon guidance, sorting, branching, and targeting in *Drosophila* brain[18,22–25]. Dscam1-mediated repulsion underlies axonal branch segregation[26] and axonal projection into different target areas[27]. Thus, Fly Dscam1 is essential for isoneuronal self-avoidance for neural circuit formation. In contrast to Dscam1, Fly Dscam2 has only two isoforms differing at Ig7, and mediates axonal tiling in the *Drosophila* visual system, suggesting that Dscam2 regulates both isoneuronal and homotypic self-avoidance[16].

However, the role of Dscam1 in cell identity code for self/non-self discrimination in *Drosophila* is fulfilled by clustered Protocadherins in vertebrates[15]. Vertebrate genomes contain only two *Dscam* genes, *Dscam* and *DscamL1*, without extensive alternative splicing[15]. In mouse *Dscam* and *DscamL1* mutant retina, neurite arborization and mosaic spacing of cell bodies are compromised, leading to excessive self-crossed neurites and clumped cell bodies of the same cell subtypes[17,28]. So, mouse DSCAMs regulate homotypic avoidance, in a manner similar to *Drosophila* Dscam2. However, in contrast to *Drosophila* Dscam1/2-mediated active repulsion in self-avoidance, mouse DSCAMs are likely to serve as non-stick coatings that mask cell-type-intrinsic adhesive cues, rather than activating repulsion[29,30]. Indeed, DSCAM promotes self-avoidance of neurites of the same cell-types by masking the functions of cadherin family members in mouse retina[29]. However, compared with the neurite avoidance mechanism, DSCAM-mediated mosaic soma spacing of the same cell-type has not been intensively studied.

Here, we showed that one of zebrafish Dscams, Dscamb, is essential for cone mosaic formation in zebrafish. In *dscamb* mutant retinas, four cone cell-types fail to form the regular mosaic pattern in either the embryonic or adult stage, especially leading to abnormal clustering of red cones. So, we focused on red cones for their mosaic spacing. *dscamb* mRNA is transiently expressed in early stages of photoreceptor differentiation, and GFP-tagged Dscamb is localized in the apical domain, including filopodium-like neurites of cone photoreceptors. Interestingly, red cones actively extend apical filopodia to apical surfaces of surrounding cones, but promptly retract them once they contact neighboring red cones. However, in *dscamb* mutants, red cone filopodia do not retract, but continue growing on apical surfaces of neighboring red cones, suggesting that apical filopodium-mediated homotypic recognition and contact-dependent filopodial retraction underlie red cone mosaic spacing in a Dscamb-dependent manner. Finally, in vivo time-lapse imaging and computational simulation support a model in which contact-dependent retraction of filopodia from the same cone type promotes their homotypic self-avoidance movement, leading to acquisition of cone spacing regularity. Thus, we conclude that Dscamb is essential for cone mosaic formation in zebrafish.

Results

The cone mosaic pattern is disrupted in zebrafish *dscamb* mutants

In zebrafish, three *dscam* genes, *dscama*, *dscamb*, and *dscaml1*, have been identified, and only *dscamb* mRNA is expressed in zebrafish retinal photoreceptors[31]. We investigated the role of zebrafish *dscamb* in cone mosaic formation. Using CRISPR/Cas9 genome editing, we generated two zebrafish *dscamb* mutant alleles, namely *dscamb*[oki9] and *dscamb*[oki10], which carry 1 base- and 10-base deletions, respectively (Supplementary Fig. 1). Both deletions cause a 1-base shift of the open reading frame in exon 4, which generates a premature termination codon after an additional 28 and 26 amino acids, respectively, in the extracellular Ig2 domain. Consistently, both *dscamb*[oki9] and *dscamb*[oki10] mutants showed almost the same phenotypes, so we used both alleles in this study. We also confirmed that no off-target mutation occurs in the CRISPR/Cas9-targeted exon4 of

dscama and *dscaml1* genes in either *dscamb* mutant allele (Supplementary Fig. 2a–d).

We examined the adult peripheral retina at 4 months post-fertilization (4mpf), using two transgenic strains Tg[thrb:tdTomato][9] and Tg[sws2:GFP][32], which visualize red and blue cones, respectively (Fig. 1c). Like wild type, *dscamb* heterozygous mutant retinas normally showed a regular lattice-like cone mosaic pattern, in which UV cones and pentameric cone units are alternately positioned. However, in *dscamb* homozygous mutants, this regular cone mosaic pattern was disrupted. In particular, red and blue cones showed abnormal clustering of the same cone types (Fig. 1c). In contrast, UV cones did not show homotypic clustering, but had a similar spacing, and a majority of green cones normally flanked UV cones (Fig. 1c). Consistently, homotypic contact was significantly increased in red and blue cones, but not in green and UV cones (Fig. 1d). However, we evaluated cone mosaic spacing with a regularity index, which is defined by conventional nearest neighbor distance[33]. The regularity index for all cone-types was significantly decreased in *dscamb* mutants, compared with heterozygous siblings (Fig. 1e). It is likely that abnormal clustering of red and blue cones in *dscamb* mutants disrupts the pentameric cone unit, which influences the regularity of UV and green cones, leading to a low regularity index of all cone-types. *Dscam* mutant mice exhibit excessive numbers of the same cell types in retina[17,28]. Therefore, we examined the density of each cone-type. Although UV cones show a weak reduction of density, the density of other cone-types was not altered in *dscamb* mutants (Fig. 1f). The weak reduction of UV cone density in *dscamb* mutants may be due to the disruption of pentameric cone units, which normally align the UV cone position by surrounding UV cones with blue and green cones.

Next, we examined the cone mosaic pattern in zebrafish embryonic retinas at 5 days post-fertilization (dpf) (Fig. 1b). Zpr1 antibody labels double-cone photoreceptors (red/green cones)[4] and was applied to double transgenic Tg[thrb:tdTomato][9] and Tg[sws2:GFP][32] embryos, enabling us to identify all cone-types (Fig. 1g). Although heterozygous retinas do not form the precise lattice-like cone mosaic pattern[4,34,35], all cone types show relatively normal mosaic spacing. However, red and blue cones showed abnormal clustering in *dscamb* mutants, although the clustering of blue cones was milder than that of red cones. The regularity index was significantly decreased for red, but not for other cone types in *dscamb* mutants (Fig. 1h). There was no difference in cell density for any cone type between *dscamb* mutants and heterozygous siblings (Fig. 1i). It is unlikely that Dscamb modulates cone cell number though regulation of precursor proliferation or survival. Taken together, these data suggest that Dscamb is required for cone mosaic spacing, especially red cones, in zebrafish retinas.

Dscamb protein is localized in filopodium-like neurites of cones, which tangentially extend to neighboring cones

In contrast to *Drosophila dscam1*, vertebrate *Dscam* genes lack clustered exons and do not produce an extensive number of isoforms[15]. Our sequencing of zebrafish *dscamb* cDNAs prepared from zebrafish retinas revealed only one full length isoform, although there was another isoform that harbors a 7 base-deletion, leading to a putative non-functional truncated protein carrying only the first five Ig domains (Fig. 2a). In situ hybridization of zebrafish embryos at 56 h post-fertilization (hpf) and juvenile retinas at 1.5 mpf revealed that *dscamb* mRNA was expressed in embryonic retinas and the juvenile retinal ciliary marginal zone (CMZ) where retinal stem cells continue to generate retinal neurons throughout life (Fig. 2b), suggesting that *dscamb* mRNA is expressed in early differentiating photoreceptors. In *dscamb* mutants, clustering phenotypes were more severe in red cones than in other cone-types (Fig. 1c, d, g). So, we conducted double in situ hybridization using mRNA probes of *dscamb* and a red cone marker, *thrb*. *dscamb* mRNA is expressed in both *thrb*-positive and -negative

a

b

c

d

e

f

g
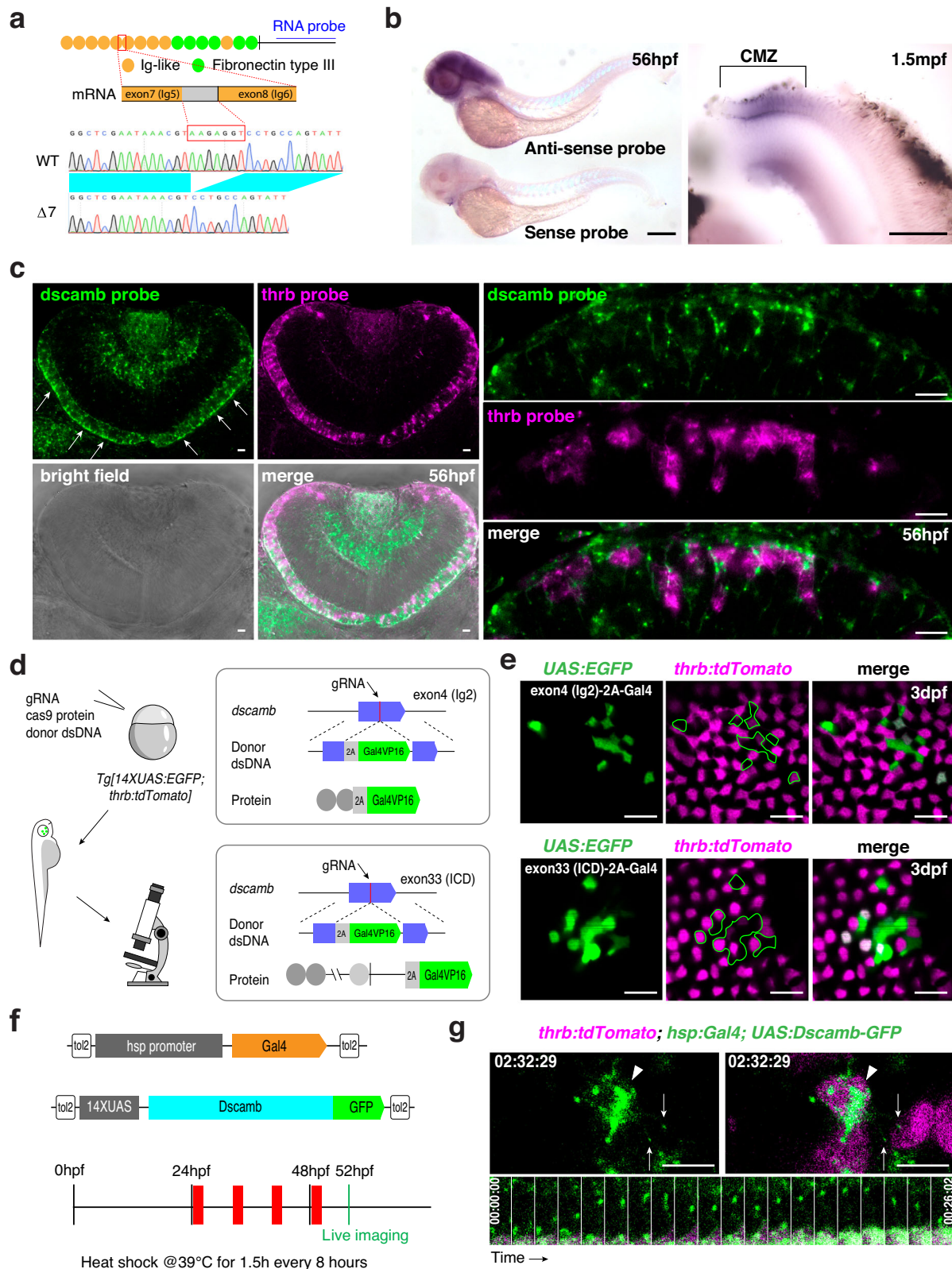
photoreceptors (Fig. 2c), suggesting that *dscamb* mRNA is expressed not only in red cones, but also other photoreceptor types. This is consistent with a previous report indicating that zebrafish Dscamb is expressed in all photoreceptors using a promoter-hijacking reporter line[36].

Since clustering phenotypes were milder in non-red cones than in red cones, it is possible that non-red cones express only the defective isoform with the 7 base-deletion in exon 7 (Fig. 2a). So, we examined whether full-length Dscamb protein is expressed in non-red cones. Using CRISPR/Cas9 mediated genome editing, we stochastically generated photoreceptors in which the DNA fragment encoding 2A-Gal4VP16 was inserted in-frame in exon 4 or exon 33 of the *dscamb* gene, in the zebrafish transgenic fish *Tg[14XUAS:EGFP; thrb:tdTomato]* (Fig. 2d). We observed expression of EGFP in

Fig. 2 | Dscamb is localized in apical filopodium-like neurites of cone photo-receptors. a Zebrafish Dscamb protein has conserved Ig-like and FNIII domains in the extracellular domain. In addition to one full-length isoform, we detected cDNA encoding a 7-bp-deletion isoform. An RNA probe is designed in the intracellular domain. **b** In situ hybridization of 56-hpf zebrafish embryos (left) and 1.5-mpf dissected retinas (right) with a *dscamb* RNA probe. *dscamb* mRNA is expressed in differentiating photoreceptors near the retinal ciliary marginal zone (CMZ). Three independent experiments. **c** In situ hybridization of 56-hpf retinas with *dscamb* (green) and *thrb* (magenta) RNA probes. *dscamb* mRNA is expressed in photoreceptor layer (white arrows in left upper panel). Higher magnification images (right panels) indicate that *dscamb* mRNA signals were detected in both *thrb*-positive (red cones) and -negative photoreceptors. Three independent experiments. **d** CRISPR/Cas9-mediated strategy of in-frame knock-in of 2A-Gal4VP16 DNA into exon 4 and exon 33 of the *dscamb* gene. **e** Mosaic generation of

photoreceptors in which 2A-Gal4VP16 DNA was inserted in-frame in exon 4 (upper panels) and exon 33 (bottom panels) of the *dscamb* gene in 3-dpf *Tg[UAS:EGFP; thrb:tdTomato]* transgenic retinas. tdTomato labels red cones. EGFP (green) was expressed in both red cones and non-red cone photoreceptors in both cases. Three independent experiments for each exon trapping. **f** Experimental design to visualize GFP-tagged Dscamb in cones. Transgenic embryos carrying *Tg[hsp:Gal4; UAS:Dscamb-GFP]* were used for live scanning at 52 hpf after multiple heat-shock treatments. **g** Live imaging of apical surfaces of red cones in transgenic embryos carrying *Tg[hsp:Gal4; UAS:Dscamb-GFP; thrb:tdTomato]* at 52 hpf. tdTomato labels red cones. GFP-tagged Dscamb was accumulated on apical domains (arrowheads) and at tips of filopodia (arrows). The time series montage (bottom panels) indicates that GFP-tagged Dscamb localization at the filopodial tip is maintained during filopodial extending/retracting cycle. Scale bars: 300 μm **b**, 10 μm **c**, **e** and 5 μm **g**.

tdTomato-negative photoreceptors regardless of whether 2A-Gal4VP16 DNA fragment was inserted into exon 4 or exon 33 (Fig. 2e). Since the non-functional isoform with the 7-base deletion generates a truncated protein carrying only the first five Ig domains, EGFP expression in exon 33-targeted knock-in photoreceptors suggests that full-length Dscamb protein is expressed in non-red cone photoreceptors. Furthermore, to explain why homotypic clustering is severe in red cones, we examined whether other *dscam* genes, namely *dscama* and *dscaml1*, are ectopically upregulated to compensate for the loss of Dscamb in non-red cone types. However, in situ hybridization showed that neither *dscama* nor *dscaml1* mRNA was expressed in the photoreceptor layer of *dscamb* mutants, similar to heterozygous siblings (Supplementary Fig. 2e).

Next, we examined its protein localization in cone photoreceptors. Unfortunately, we did not have specific antibodies against zebrafish Dscamb, so we expressed C-terminal GFP-tagged Dscamb proteins in wild-type retinas at 52 hpf using the Gal4-UAS system under the control of a heat-shock promoter (Fig. 2f). Live imaging revealed that GFP-tagged Dscamb is localized in the apical region of red cones, including filopodium-like neurites, which are extended tangentially from the apical domain (Fig. 2g, Supplementary Movie 1). It was reported that vertebrate DSCAMs have PDZ-interacting motif at the C-terminus, through which DSCAMs interact with scaffolding proteins[37,38]. To exclude the possibility that C-terminal GFP-tagging compromises the function of PDZ-interacting motif in zebrafish Dscamb, we confirmed that the N-terminal mEGFP-tagged Dscamb showed almost the same localization (Supplementary Fig. 3).

Apical cone filopodia recognize the same cone type to activate homotypic self-avoidance

After formation of the outer nuclear layer (ONL) around 40 hpf in zebrafish, photoreceptor progenitors dynamically extend and retract filopodium-like neurites, the direction of which is tangential to the apical surface, corresponding to the future position of the outer limiting membranes (OLM)[39]. Importantly, such dynamic extension behaviors of apical photoreceptor neurites are active only transiently from 40 to 60 hpf, prior to photoreceptor maturation. Transient expression of *dscamb* mRNA in differentiating photoreceptors (Fig. 2b, c) and subcellular localization of GFP-tagged Dscamb on apical filopodium-like neurites of cone photoreceptors (Fig. 2g, Supplementary Movie 1) led us to examine whether Dscamb regulates apical filopodium behavior during photoreceptor development.

To visualize apical filopodia of red cones, we combined *Tg[thrb:tdTomato]* with another transgenic line, *Tg[thrb:Gal4VP16;UAS:lifeact-GFP]*, which visualizes filamentous actin[40]. First, we scanned paraformaldehyde (PFA)-fixed wild-type and *dscamb* mutant embryonic retinas in 3D, and confirmed that red cones laterally extend multiple filopodia into the neighboring cone area at the OLM

level of photoreceptor layer (Supplementary Movie 2). Second, we carried out time-lapse live imaging of red cone filopodia at the OLM level (Fig. 3a). In the scanning image, all red cone cell bodies were labeled with tdTomato fluorescent signals; however, Lifeact-GFP was expressed only in a fraction of red cones (Fig. 3b). This stochastic expression of Lifeact-GFP was beneficial, because it enabled us to examine how apical filopodia of red cones interact with neighboring GFP-negative red cones at single-cell resolution. Interestingly, red cones actively extended filopodia until they reached cell bodies of neighboring red cones, but red cone filopodia ceased growing when they contacted apical regions of neighboring red cones in wild type (Fig. 3b, c, Supplementary Movie 3). However, in *dscamb* mutants, apical filopodia of red cones continued to grow even after they reached cell bodies of neighboring red cones and further invaded the apical domain territory (Fig. 3b, c, Supplementary Movie 3). It is likely that red cones recognize other red cones through apical filopodium-mediated physical contact, which subsequently triggers filopodial retraction. Homotypic recognition and subsequent self-avoidance between red cones are compromised in *dscamb* mutants.

To evaluate filopodium defects in *dscamb* mutants, we calculated the fraction of red cones, in which one or more filopodia invade >2 μm into the apical region of neighboring red cones within the first 1 h of live scanning. The fraction of red cones with invading filopodia was markedly higher in *dscamb* mutants than in wild-type siblings, which represent a mixture of wild-type and heterozygous embryos (Fig. 3d). Next, we developed a temporal profile of the distance between filopodium tips and the apical domain border of neighboring red cones for each filopodium (Supplementary Fig. 4). The maximum invading distance was longer in *dscamb* mutants than in wild-type siblings (Fig. 3e). The maximum filopodium length was also greater in *dscamb* mutants than in wild-type siblings (Fig. 3f). Furthermore, compared with *dscamb* mutants, wild-type sibling filopodial tips spent more time at the border of neighboring red cones (Fig. 3g). Thus, extension, pausing, and retraction of red cone filopodia represent the recognition process between red cones, which probably depends on homophilic interaction of Dscamb between apical filopodia and neighboring cones. Next, we examined the residence duration of red cone filopodia on the apical regions of neighboring cones. To minimize sampling variation caused by the initial distance between filopodia-extending and -targeting cones, we selected filopodium-targeting cones that did not directly contact the filopodium-extending red cone but were closely positioned at the distance around one cell size at the beginning of measurement. First, we examined homotypic contact of red cone filopodia in *dscamb* mutants. Compared with wild-type siblings, *dscamb* mutant red cone filopodia spend more time on the apical regions of neighboring red cones (Fig. 3h), suggesting that retraction failure of red cone filopodia from neighboring red cones correlates with the longer duration of red cone filopodia on neighboring red cones in *dscamb* mutants. Second, we evaluate homotypic and heterotypic contact of
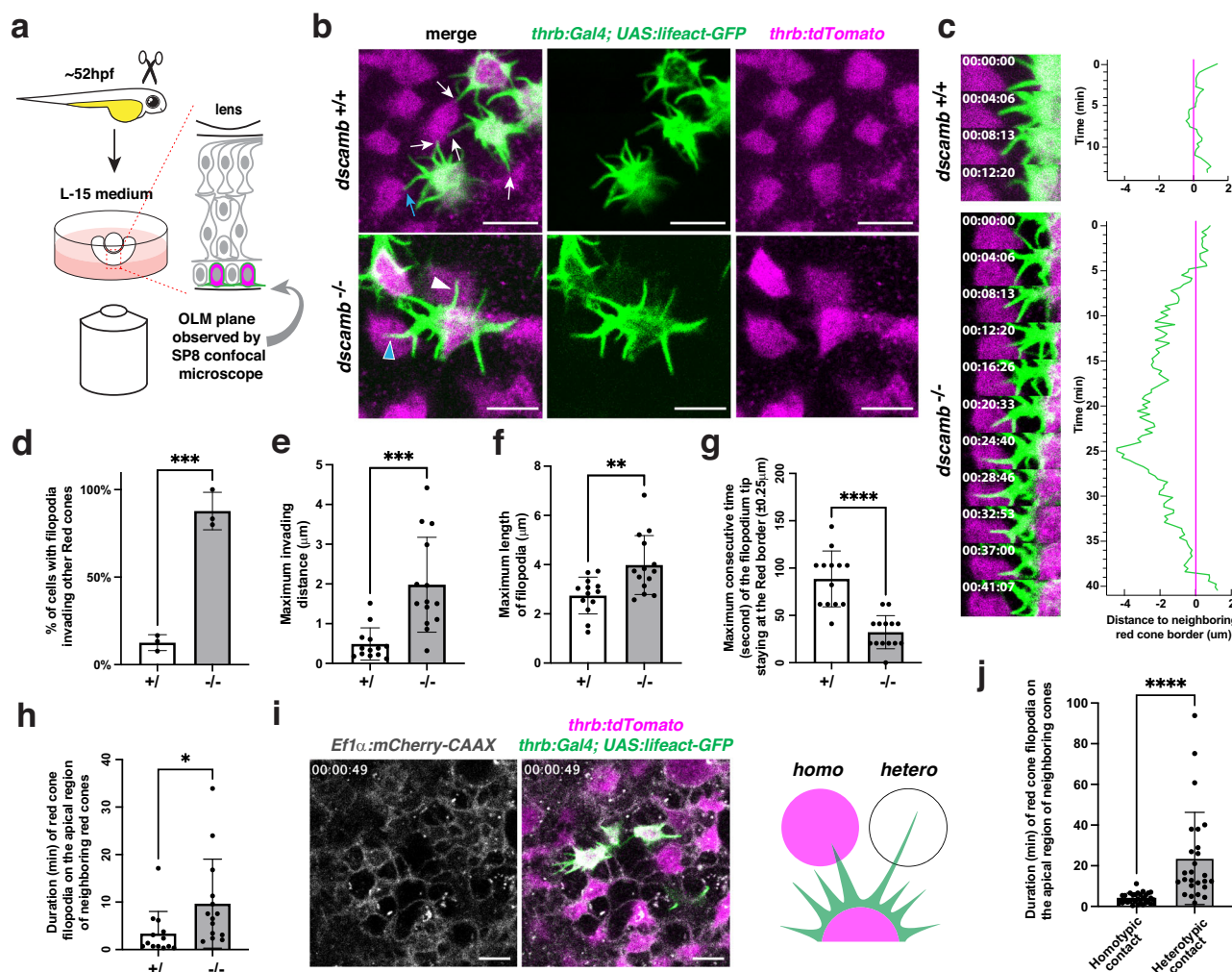
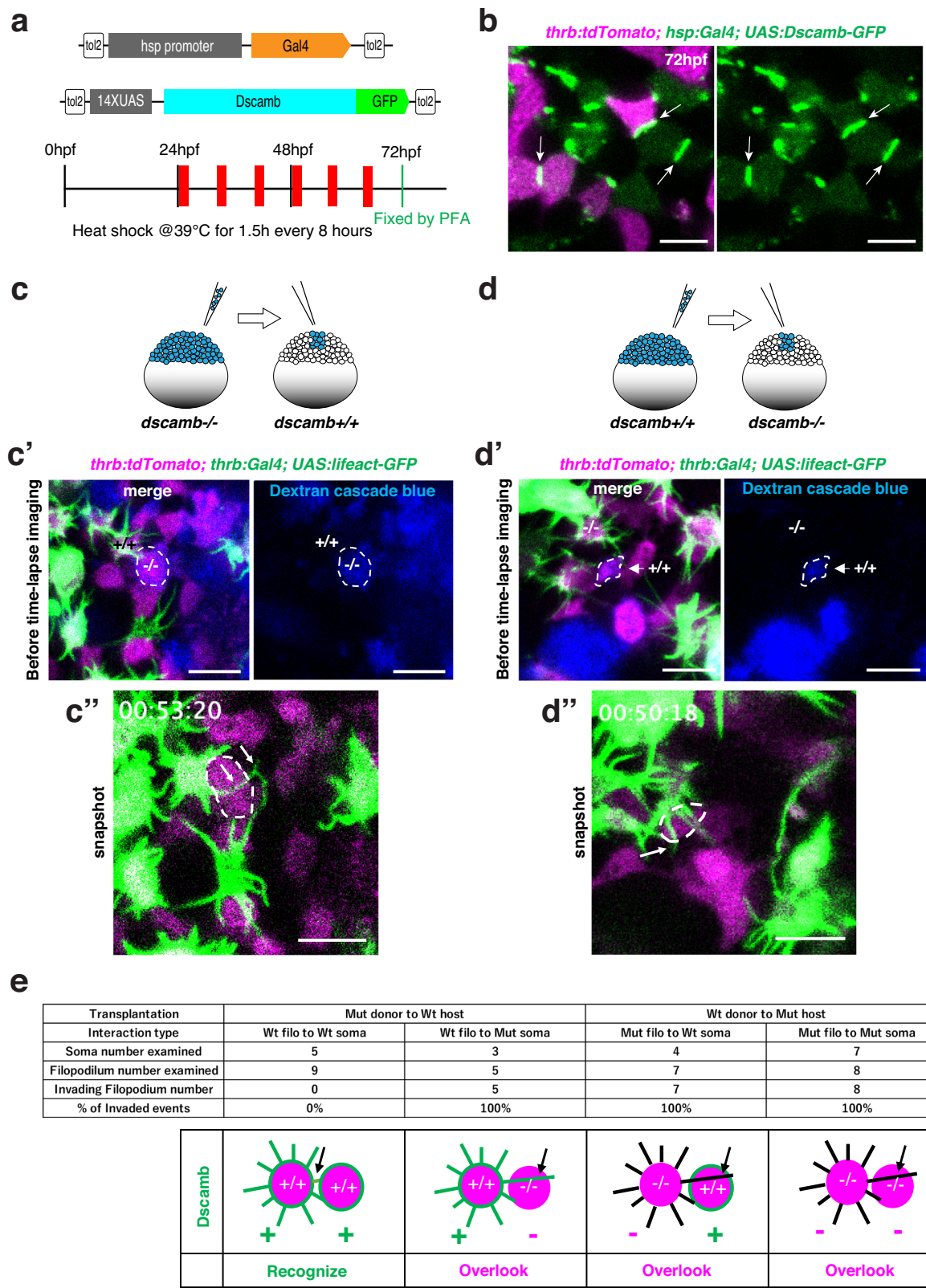**Fig. 3 | Dscamb is required for filopodium-mediated homotypic recognition.**
a Experimental design for ex vivo live imaging. OLM: outer limiting membrane.
b Confocal images of the apical surface of a cone photoreceptor layer with two transgenes *Tg[thrb:Gal4VP16; UAS:lifeact-GFP]* and *Tg[thrb:tdTomato]*, which visualize apical filopodia (green) and cell bodies (magenta) of red cones, respectively. In wild type, red cones extend multiple filopodia toward neighboring cones. However, filopodia stop growing when they meet neighboring red cones (white/blue arrows). On the other hand, in *dscamb* mutants, filopodia keep growing even after they contact other red cones (white/blue arrowheads). A blue arrow and arrowhead indicate wild-type and *dscamb* mutant filopodia used for time-lapse analysis shown in the panel **c**. Three independent experiments. **c** Time-lapse observation of filopodial behavior in wild-type and *dscamb* mutant red cones. Right histograms show a temporal profile of the distance between a filopodial tip and an apical domain border of neighboring red cones, which was measured every 20.6 s. **d** Percentage of red cones with invading filopodia. **e** Maximum invading distance of apical filopodia. **f** Maximum length of apical filopodia. **g** Maximum consecutive

time of filopodium tip staying within the border zone (± 0.25 μm) of the apical domain of red cones. **h** Residence time of red cone filopodia on apical domains of neighboring red cones. **i** Confocal scanning of the photoreceptor layer in triple transgenic *Tg[thrb:Gal4VP16; UAS:lifeact-GFP; Ef1α:mCherry-CAAX]* retinas, which visualize red cone filopodia (green) contacting on other red cones (homotypic, magenta) or other non-red cone-type photoreceptors (heterotypic, white).
j Residence time of red cone filopodia (collected from 3 wild-type samples) on apical domains of other red cones (homotypic contact) or other non-red cone-type photoreceptors (heterotypic contact). **d**–**h**, **j** Means ± SD. Statistical significance was evaluated with unpaired t-tests (two tail): *p < 0.0332, **p < 0.0021, ***p < 0.0002, and ****p < 0.0001. Biological replicates: **d** Three embryos. **e**–**h** n = 13 for wild-type filopodia and n = 14 for *dscamb* mutant filopodia. **j** n = 30 for filopodia showing homotypic contact and n = 26 for filopodia showing heterotypic contact. Scale bars: 5 μm **b**, **i**. **d**–**h**, **j** Source data and p-values are provided as Source Data for Fig. 3.

red cone filopodia in wild-type embryos. We combined *Tg[thrb:Gal4VP16;UAS:lifeact-GFP]* with another fish strain *Tg[Ef1a:mCherry-CAAX]*, which visualizes the plasma membrane outline, and we calculated the residence duration of red cone filopodia on the apical regions of red cones and other photoreceptor types (Fig. 3i). Wild-type red cone filopodia stay more than 5 times longer on apical regions of other surrounding photoreceptor types than on apical domains of proximal red cones after they encounter (Fig. 3j). These data suggest that the residence duration of red cone filopodia on neighboring cones is much longer for heterotypic contact than for homotypic contact.

Homotypic avoidance of red cones requires homophilic interaction of Dscamb

We investigated whether Dscamb is required in both filopodia tips and neighboring red cones for filopodium-mediated homotypic recognition. First, we expressed GFP-tagged Dscamb, using the Gal4-UAS system under the control of a heat-shock promoter (Fig. 4a). Dscamb-GFP accumulated at the interface between GFP-positive cells (Fig. 4b), suggesting intercellular, homophilic interaction of Dscamb. Second, we conducted cell transplantation experiments. When *dscamb* mutant donor cells were transplanted into wild-type host embryos (Fig. 4c), a wild-type red cone extended its filopodia, which

Transplantation	Mut donor to Wt host		Wt donor to Mut host	
Interaction type	Wt filo to Wt soma	Wt filo to Mut soma	Mut filo to Wt soma	Mut filo to Mut soma
Soma number examined	5	3	4	7
Filopodium number examined	9	5	7	8
Invading Filopodium number	0	5	7	8
% of Invaded events	0%	100%	100%	100%

did not stop at the border of a neighboring *dscamb* mutant red cone, but continued to extend to its apical domain (Fig. 4c', c", Supplementary Movie 4). When wild-type donor cells were transplanted into *dscamb* mutant host embryos (Fig. 4d), a *dscamb* mutant host red cone extended filopodia, which overshot the apical domain of wild-type donor red cones (Fig. 4d', d", Supplementary Movie 5). Thus, only when Dscamb is present on both filopodia and neighboring red

cones, can filopodium-mediated homotypic recognition and subsequent self-avoidance be achieved (Fig. 4e).

Filopodium-mediated homotypic avoidance also occurs between blue cones

Next, we examined whether filopodium-mediated homotypic recognition and self-avoidance occurs in other cone types, especially blue

Fig. 4 | Filopodium-mediated homotypic recognition requires homophilic interaction of Dscamb. a Experimental design to visualize Dscamb-GFP protein in cones at 72 hpf. **b** Confocal imaging of the ONL of *Tg[thrb:tdTomato; hsp:Gal4; UAS:Dscamb-GFP]* transgenic retinas. Dscamb-GFP was localized to the interface between GFP-positive cells (arrows). Three independent experiments. **c, d** Cell transplantation experiments with *dscamb* mutant donor cells in wild-type host retinas **c** and vice vasa **d**. Both donor and host embryos carry *Tg[thrb:tdTomato]* to visualize all the red cones (magenta). At least, either donor or host embryos carries *Tg[thrb:Gal4VP16; UAS: lifeact-GFP]* to visualize filopodia of red cones (green). Donor cells were injected with Dextran cascade blue (blue) at the 1-cell stage and transplanted into host embryos at the blastula stage to generate chimeric retinas at 52 hpf. **c', d'** Before time-lapse scanning, we selected a single donor red cone (dotted outline), which had both thrb:tdTomato and Dextran cascade blue and was

also close to host red cones expressing both thrb:tdTomato and Lifeact-GFP. Biological replicates are indicated by sample size shown in **e. c'', d''** Extension behaviors of Lifeact-GFP-labeled host filopodia to a donor red cone after around 1 h time-lapse scanning. In both transplantation from mutant donor to wild-type host **c''** and from wild-type donor to mutant host **d''**, filopodia of the host red cone (arrow) invade the apical domain of the donor red cone (dotted outline). **e** Summary of transplantation results. The upper table indicates the sample size and the percentage of filopodial invaded events for each donor-host combination. The lower schematic drawing indicates that filopodia (black arrows) of red cones (magenta) stop their extension to neighboring red cones, only when both filopodia-extending red cones and targeting red cones express Dscamb (green). Scale bars: 5 µm **b, c'-c'', d'-d''**.

cones, because blue cones are abnormally clustered in *dscamb* mutants (Fig. 1c, g). To visualize blue cones and their precursors, we generated a zebrafish transgenic line, *Tg[foxq2-2A-Gal4VP16; UAS:EGFP]*, in which a DNA fragment of *2A-Gal4VP16* was inserted into exon 2 of the *foxq2* gene (Supplementary Fig. 5a). We confirmed that EGFP-positive cone precursor cells undergo symmetric terminal division to produce twin blue cones (Supplementary Fig. 5b, Supplementary Movie 6). Next, we combined *Tg[foxq2-2A-Gal4VP16; UAS:EGFP]* with *Tg[thrb:tdTomato]* to examine whether blue cones recognize neighboring red cones, or with *Tg[UAS:lifeact-mCherry]* to examine whether blue cones recognize neighboring blue cones. Indeed, blue cones extend their filopodia, which continue to grow over apical domains of neighboring red cones (Supplementary Fig. 5c, Supplementary Movie 7), but stop growing at neighboring blue cones (Supplementary Fig. 5d, Supplementary Movie 8), indicating similar apical filopodium-mediated, homotypic recognition of blue cones. Surprisingly, this homotypic recognition and subsequent retraction of blue cone filopodia from neighboring blue cones were normal in *dscamb* mutants, similar to heterozygous siblings (Supplementary Fig. 5e, Supplementary Movie 9), suggesting that Dscamb is dispensable for homotypic recognition and subsequent avoidance between blue cones.

Filopodium-mediated, homotypic avoidance promotes mosaic spacing of red cones

Recognition of neighboring red cones by red cone filopodia triggers retraction of red cone filopodia from neighboring red cones, resulting in shorter residence of filopodia on apical domains of neighboring red cones than on apical domains of non-red cones. We hypothesized that this shorter duration promotes avoidance movement between red cones, resulting in spatial segregation of red cones. Indeed, our time-lapse imaging of cone behaviors in *Tg[thrb:tdTomato; thrb:Gal4VP16; UAS:lifeact-GFP]* retinas revealed that in wild type, new-born red cones extend filopodia toward spaces that red cones do not occupy, but do not extend filopodia to apical domains of neighboring red cones, which apparently allows the filopodium-extending red cone to move away from nearby red cones, resulting in physical separation of red cones (Fig. 5a, and Supplementary Movie 10). In *dscamb* mutants, red cones intensively extend filopodia to apical domains of neighboring red cones, which seems to suppress self-spacing behavior, resulting in formation of red cone clusters (Fig. 5a, Supplementary Movie 10).

To evaluate the physical separation process between red cones, we focused on red cone precursors that give rise to twin red cones and determined the fraction of cells contacted by other red cones in initial red-cone precursors and later red-cone progeny (Fig. 5b). The fraction of red cone precursors contacted by other red cones at metaphase of mitosis (t = 0) was 66.7% (= 14/21) and 73.1% (= 19/26) in wild type and *dscamb* mutants, respectively, which was statistically non-significant. However, the fraction of red cone progeny contacted by other red cones 5 h after mitosis was 23.8% (= 10/42) and 69.2% (= 36/52) in wild

type and *dscamb* mutants, respectively, indicating that physical separation between red cones proceeds more efficiently in wild type than in *dscamb* mutants. Thus, spatial segregation between red cones is achieved during the period with active extension of cone filopodia in a Dscamb-dependent manner.

Next, to determine whether the regularity of red cone spacing is progressively achieved during the period with active extension of cone filopodia, we monitored the spatial pattern of red cones by time-lapse imaging of the ONL of *Tg[thrb:tdTomato]* transgenic retinas after 52 hpf (Fig. 5c). In wild-type ONL at 52 hpf, red cones and their progenitors showed less regular spacing with cell clustering. However, after 12 h, red cones segregated to achieve more regular spacing in wild type (Fig. 5c, Supplementary Movie 11). On the other hand, such a transition to regular spacing was not clearly observed in *dscamb* mutants, and numerous red cones were still clustered after 12 h (Fig. 5c, Supplementary Movie 11). Next, we developed a temporal profile on the regularity index (Fig. 5d). The regularity index of red cones in the last 1 h of the scanning period was significantly higher than during the first 1 h in wild type, whereas there was no significant difference between the first and the last 1 h of the scanning period in *dscamb* mutants (Fig. 5e). Thus, a regular mosaic spacing of red cones is progressively established during the cone filopodium active period in a Dscamb-dependent manner.

To further confirm that filopodial contact-dependent avoidance movement between homotypic cones is essential for regular mosaic spacing, we applied computer simulation under conditions that mimic red cone behavior in wild type and *dscamb* mutants. This simulation was conducted on three mechanical assumptions. First, red cones have filopodia that can extend and retract. Second, longer filopodia receive stronger pulling force during retraction, leading to cell movement. Third, filopodia stop growing and retract once their tips meet nearby red cones, which is suppressed in the mutant condition. Based on the above assumptions, wild-type, red cones receive pulling forces only from non-red cones, biasing their migratory direction toward non-red cone areas, whereas in *dscamb* mutants, red cones are pulled toward both surrounding red and non-red cones, leading to no bias of migratory direction (Fig. 5f). In a simulation of wild-type conditions, red cone spacing changed from an initial random pattern into a more regular pattern, whereas red cone spacing remained disordered at the end of the simulation of *dscamb* mutants (Fig. 5g, Supplementary Movie 12). In this simulation, the regularity index of the wild-type condition progressively increased to 6.22 (Fig. 5h), which is similar to the regularity index of in vivo measurements (5.92) (Fig. 5d). In contrast, the regularity index of the *dscamb* mutant condition remains low (2.59) (Fig. 5h). The regularity index of red cones in the last 100 frames of the simulation was significantly higher than that of the first 100 frames in the wild-type condition, whereas there was no significant difference between the first and the last 100 frames of the simulation in *dscamb* mutants (Fig. 5i). Thus, filopodial contact-dependent, homotypic avoidance can explain progressive establishment of the regular spacing of red cones during the cone filopodium-active period.
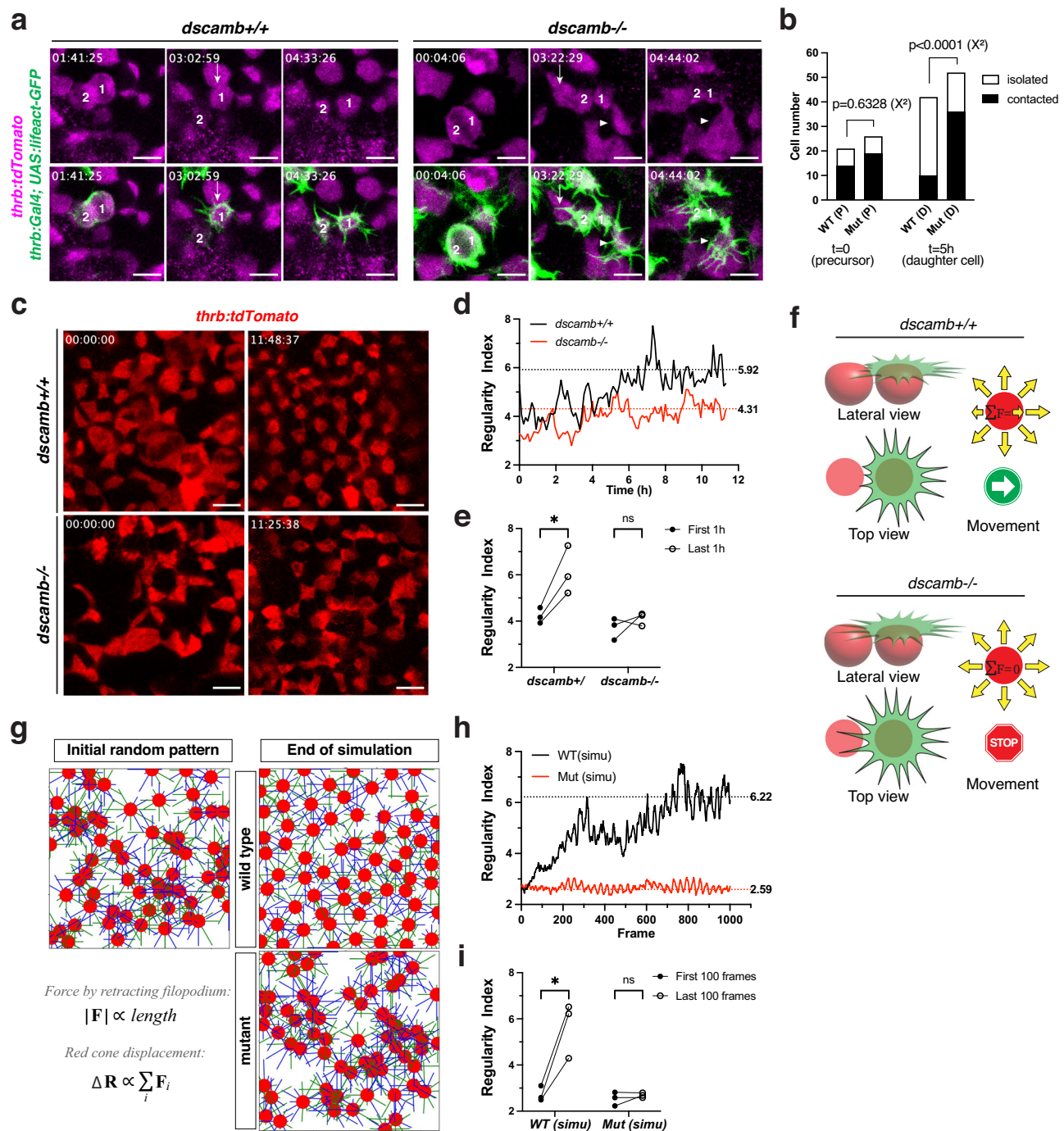
Fig. 5 | Filopodium-mediated avoidance movement promotes mosaic spacing of red cones. a Time-lapse imaging of twin red cones in *Tg[thrb:Gal4VP16; UAS:lifeact-GFP; thrb:tdTomato]* transgenic retinas. The top row indicates the magenta channel (*thrb:tdTomato*). Lifeact-GFP-expressing twin red cones arise by progenitor division (each left panel). Their filopodia avoid neighboring red cones in wild-type, but grow into neighboring red cones in *dscamb* mutants (each middle panel, arrow). Twin red cones progressively separate from each other and from other red cones in wild-type, but remain associated with each other and with other red cones in mutants (each right panel). A red cone used filopodia to associate with other red cones (middle and right panels of mutant, arrowhead). **b** Numbers of red cone progenitor cells (P) and their red cone progeny (D), which are contacted by (black bars) or isolated from other red cones (white bars). Statistical difference was evaluated with the chi-square test (two tail). **c** Twelve-hour time-lapse scanning of red cone spacing in *Tg[thrb:tdTomato]* transgenic retinas after 52 hpf. **d** Temporal

profile of the regularity index of red cones, shown in panel **c**. Dashed lines represent the mean of the regularity index of the last 1 h. **e** Comparison of mean regularity indices of the first and last one hour. Three biological replicates. Statistical significance was evaluated with paired t-test (two tailed): *p < 0.05, ns: not significant. **f** A model for mechanical regulation of cone movement, in which each cone may receive pulling force through its apical filopodia anchored to neighboring cones. **g** Computer simulation of red cone spacing based on the mechanical model shown in **f. h** Temporal profile of the regularity index of red cones, shown in **g**. Dashed lines represent the mean of the regularity index of the last 100 frames.
i Comparison of mean regularity indices between the first and last 100 frames. Three technical replicates for computer simulation including an initial random setting for cone mosaic pattern, filopodial length and movement. Paired t-tests (two tailed): *p < 0.05, ns: not significant. Scale bars: 5 μm **a, c**. Source data and p-values **b, e, i** are provided as Source Data for Fig. 5.

In addition, we took account of homophilic binding of Dscamb between filopodial tips and neighboring cones by setting another parameter, the slowing down coefficient (slc), which reduces filopodial retraction speed when tips of red cone filopodia are positioned inside the apical domains of neighboring red cones (Supplementary Fig. 6a). We considered three different slc conditions: (1) non-sticky tips (slc=1), (2) intermediate sticky tips (slc=0.3), and (3) very sticky tips (slc=0.15), which were applied to the computer simulation above (Supplementary Fig. 6b). Interestingly, the average nearest neighbor distance (NND) between red cones was reduced if filopodial tips were sticky (slc<1) (Supplementary Fig. 6b, c). The lower the slc was, the closer the spacing became. Unexpectedly, the regularity index of red cone spacing was higher with the intermediate sticky tips than either with non-sticky tips or very sticky tips (Supplementary Fig. 6d). Thus, Dscamb-mediated adhesion between filopodial tips and neighboring cones may determine the appropriate range of regularity and density of cone mosaic spacing by coupling with contact-dependent filopodial retraction.

Dscamb regulates the cone mosaic pattern in the pre-column zone of adult retinas

Finally, we examined whether filopodium-mediated homotypic avoidance regulates adult cone mosaic formation. In the CMZ of adult zebrafish retinas, retinal stem cells produce retinal progenitors to form the progenitor proliferating zone. Next, the pre-column zone appears, in which four cone types are positioned to form a regular cone pattern[41]. Then, pentameric cone units are formed, which alternate with UV cones to form the mature cone lattice zone. At 3 weeks post-fertilization (wpf), zebrafish red cones extend filopodia tangentially in the retinal CMZ to form the filopodium active zone, which is located just peripheral to the pre-column zone (Fig. 6a, Supplementary Movie 13). Next, we examined the cone mosaic pattern in the retinal CMZ of *dscamb* mutants and heterozygous siblings at 18 dpf. In the pre-column zone of heterozygous siblings, differentiating blue cones normally appear between red cones to form pentameric cone units (Supplementary Fig. 7a-a', Supplementary Movie 14). However, red cones were abnormally clustered to eject blue cones from pentameric cone units in the pre-column zone of *dscamb* mutants (Supplementary Fig. 7b-b', Supplementary Movie 14). Furthermore, to more precisely compare the spatial pattern of red cones in the pre-column zone, we stochastically generated *dscamb* mutant cone photoreceptors in a mosaic manner in the CMZ of 1.5 mpf juvenile retinas, using CRISPR/Cas9 genome editing (Fig. 6b). The regular cone pattern fails to form in the pre-column zone in the *dscamb* mutant area (Fig. 6b'-b"). These data suggest that Dscamb is required for a regular cone pattern in the pre-column zone by filopodium-mediated, homotypic avoidance.

In the pre-column zone, Müller cells start to differentiate, extend their apical processes, and form adherens junctions with surrounding cones. A circumferentially polarized pulling tension increases in the retinal CMZ after the larval stage and promotes the formation of the lattice-like cone mosaic pattern by mechanical regulation through adherens junctions between Müller cells and cones in the pre-column zone[41,42]. Indeed, in the CMZ in *Tg[thrb:tdTomato; gfap:GFP]* transgenic fish at 18 dpf, Müller cells start to differentiate at the interface between the filopodium active zone and the pre-column zone (Fig. 6c). In the mature cone lattice zone, N-cadherin signals normally accumulate on the apical surface around pentameric cone units, and represent adherens junctions between Müller cells and cones (Supplementary Fig. 8a-a'). However, in *dscamb* mutants, such N-cadherin signal accumulation was not observed, suggesting that Dscamb-mediated homotypic cone spacing is required for Müller cell-mediated mechanical regulation to form the mature cone lattice zone (Supplementary Fig. 8a-a'). We also conducted labeling of the mature cone lattice zone with anti-Crb2b antibody and the transgene

Tg[gnat2:ponli-GFP], whose signals are localized at the interface between cones of pentameric cone units (Supplementary Fig. 8b-c). In *dscamb* mutants, Crb2b and Ponli-GFP are localized at the interface between cones of pentameric cone units, although those cone units were deformed, suggesting that subcellular localization of Crb2b and Ponli in pentameric cone units is independent of Dscamb functions. Thus, Dscamb promotes mosaic spacing of homotypic cones in the pre-column zone, which facilitates Müller cell-mediated mechanical regulation to form the lattice-like cone mosaic pattern.

Discussion

In vertebrate retinas, different cone types form a regular spacing pattern called the cone mosaic[1]. Research on the cone mosaic in vertebrates has a long history, which was probably initiated by the first report on "Mikroskopiske Undersögelser af Nervesystemet" by Adolph Hannover in 1842, followed later by more detailed descriptions[43,44]. However, molecules that directly regulate the formation of the cone mosaic pattern have not been identified. In this study, we discovered that Dscamb regulates cone mosaic formation in zebrafish embryonic and adult retinas.

In zebrafish *dscamb* mutants, cone mosaic formation is disrupted; however, red cones show more severe defects in mosaic spacing, compared with other cone-types. Accordingly, in this study, we focused on the role of Dscamb in mosaic spacing of red cones. In zebrafish, photoreceptor progenitors or new-born photoreceptors dynamically extend and retract filopodium-like processes, whose direction is tangential to the apical surface, during early stages of photoreceptor differentiation[39]. In later stages of zebrafish photoreceptor differentiation, substantial remodeling of photoreceptor apical domains occurs to promote the transition from these tangential filopodium-like processes to vertically oriented microvilli-like calyceal processes, which are finally associated with outer segments of photoreceptors[45]. Unexpectedly, we found that GFP-tagged Dscamb is localized in the apical domain of cone photoreceptors, including filopodium-like processes. Furthermore, red cones recognize the same cone type through apical filopodium-mediated sensing of apical domains of surrounding cones. Thus, our discovery of filopodium-mediated homotypic recognition revealed an unexpected role of early tangential cone filopodia in cone mosaic formation. In general, DSCAM promotes self-avoidance of dendrites and cell bodies by homophilic binding during nervous system development[15,17,28]. Consistently, in wild-type zebrafish retinas, red cone filopodia stop growing and start to retract when they meet neighboring red cones, but continue interacting with non-red cone apical domains. Thus, filopodium-mediated homotypic recognition triggers self-avoidance of filopodia from the same cone-type. Importantly, filopodium-mediated homotypic cone recognition requires homophilic interaction of Dscamb between apical filopodia of sensing cones and apical domains of targeted cones. The homophilic interaction of Dscamb is integral to the filopodium-mediated homotypic recognition mechanism.

Homotypic spacing of other retinal neurons, such as amacrine and horizontal cells, is achieved through the tiling-like mechanism that excludes somata from the dendritic territory of neighboring homotypic neurons[46,47]. However, retinal photoreceptors are columnar cells without conventional dendrites, so how the same cone-type maintain regular spacing during cone mosaic formation has been something of a mystery. One hypothesis is that differential adhesive activity between homotypic and heterotypic cones functions in spatial segregation of homotypic cone-type during cone mosaic formation[34,48]; however, direct in vivo evidence has not been demonstrated. Our time-lapse imaging revealed that regular mosaic spacing of red cones is progressively established during the filopodium-active period. In this process, red cone filopodia normally stay longer on apical domains of neighboring non-red cones than on those of neighboring red cones, suggesting that longer anchoring of red cone filopodia to neighboring
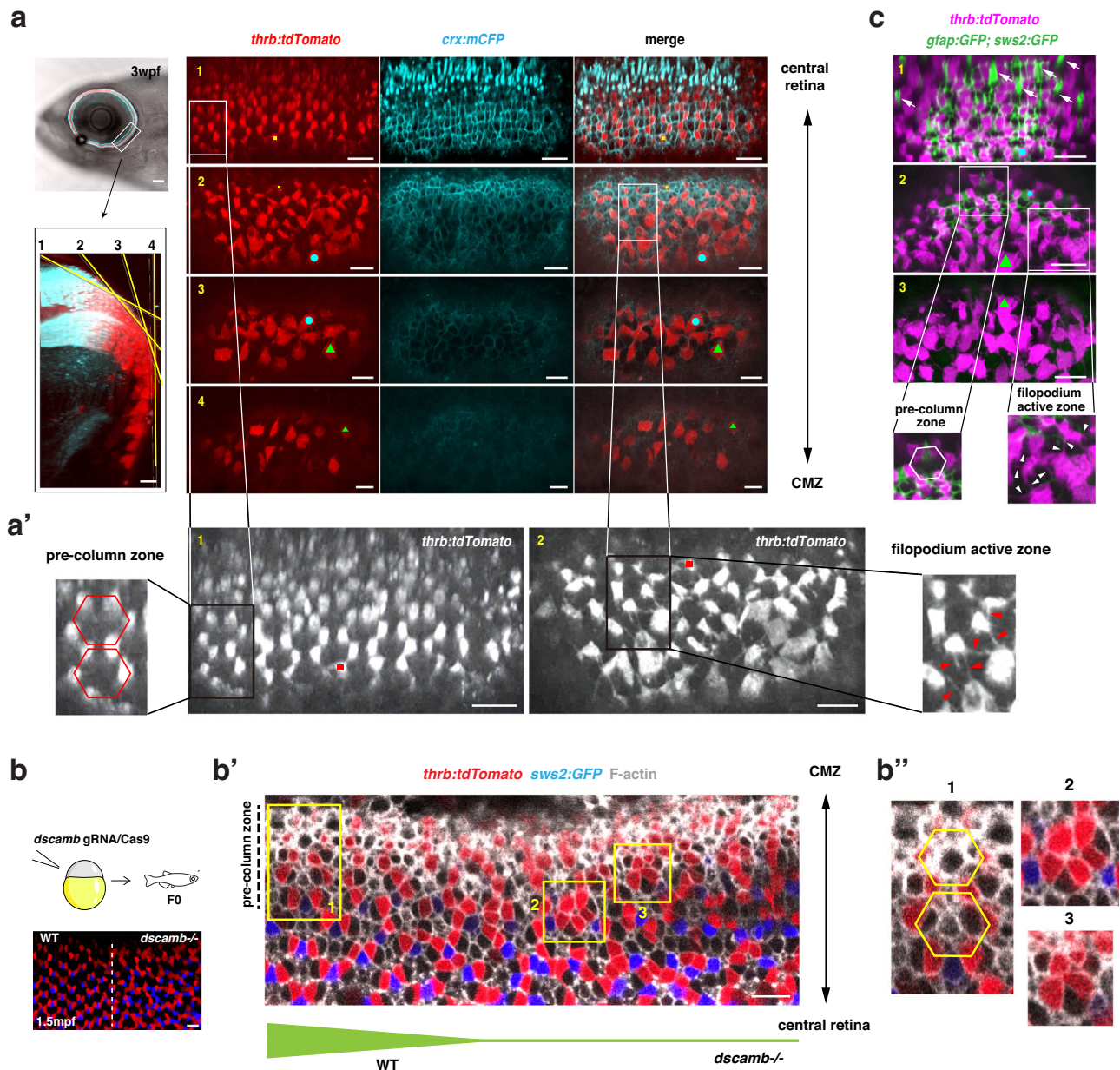
Fig. 6 | Dscamb regulates cone mosaic pattern in the pre-column zone of adult retinas. a Retinal ciliary marginal zone (CMZ) of *Tg[thrb:tdTomato; crx:mCFP]* transgenic fish at 3 wpf. Using the ventro-temporal retinal CMZ (square in the upper left panel), four overlapping tangential sections covering the apical surface from central (section 1) to peripheral (section 4) direction are scanned. Red cones and plasma membranes are shown in tdTomato (red) and mCFP (cyan) fluorescence, respectively. Small geometric landmarks adjust the overlapping position. **a'** Higher magnification of tdTomato fluorescent images of sections 1 and 2, shown in **a**. In section 1, differentiating red cones form a hexagonal pattern, indicating the pre-column zone. In section 2, the filopodium active zone, where red cones extend multiple filopodia (red arrowheads), forms just peripheral to the pre-column zone. **b** Generation of the *dscamb* mutant area in the retinal CMZs of *Tg[thrb:tdTomato; sws2:GFP]* transgenic wild-type fish at 1.5 mpf (upper panels). In the peripheral retina, a regular lattice cone mosaic is formed on the left side, whereas the *dscamb* mutant area showing red cone clustering is induced on the right side (bottom

panel). **b'** Higher magnification of the CMZ of wild-type and *dscamb* mutant chimeric retinas. Phalloidin labeling visualizes F-actin (white). Square 1 and squares 2/3 are selected from the pre-column zone of wild-type and *dscamb* mutant areas, respectively. Thickness of the bottom green line indicates presumptive Dscamb activity. **b''** Higher magnification of square 1-3 shown in **b'**. Square 1 indicates a hexagonal pattern of red cones. Squares 2/3 indicate red cone clustering. **c** Retinal CMZ in *Tg[thrb:tdTomato; gfap:GFP; sws2:GFP]* transgenic fish at 18 dpf. Three overlapping tangential sections (section 1-3) cover retinal CMZs. Small geometric landmarks adjust the overlapping position. Differentiating blue cones (white arrows) appear in Section 1. Section 2 contains the pre-column zone and the filopodium-active zone. In the latter, red cones extend multiple filopodia (white arrowheads). gfap:GFP starts to be expressed at the interface between the filopodium-active zone and the pre-column zone. **a–c** Three independent experiments. Scale bars are 10 μm **a–c**, except 100 μm for the upper left image in (**a**).

non-red cones produces a pulling force that links surrounding non-red cones to filopodia-extending red cones. On the other hand, homophilic binding of Dscamb suppresses filopodium-mediated anchoring between red cones, which allows red cones to separate. Our simulation experiments demonstrate that anisotropic pulling force biased toward

non-red cone territory contributes to the progressive separation of red cones. Furthermore, our simulation raises another interesting possibility that Dscamb-mediated adhesion between filopodial tips and neighboring cones can modulate the range of regularity and density of cone mosaic spacing. Although we have not shown in vivo evidence to

support this idea, Dscamb may determine the appropriate range of cone density and regularity by modulating the balance between adhesion and repulsion for filopodium-mediated interaction to homotypic cones. Thus, Dscamb-mediated homotypic recognition may couple with mechanical force-mediated heterotypic cone anchoring to trigger a progressive avoidance of homotypic cones, which is unique among self-avoidance mechanisms in nervous system development.

Dscamb-mediated homotypic recognition and subsequent avoidance movement between red cones could well explain progressive establishment of red cone mosaic spacing. However, in *dscamb* mutants, there was no homotypic contact of UV and green cones, and clumped phenotypes of blue cones were weaker than those of red cones. Although we and other groups suggested that *dscamb* mRNA is likely expressed in non-red cone type photoreceptors[36], it is unclear why mosaic spacing defects are absent or weak in non-red cones. Since *dscamb* gene transcribes the full-length isoform as well as the defective isoform with a 7 base-deletion in exon 7, it is possible that non-red cones express only this defective isoform. However, photoreceptors with in-frame knock-in of the DNA construct encoding 2A-Gal4VP16 in exon 33 of the *dscamb* gene revealed that the full-length isoform is normally expressed in both red and non-red cone types. Furthermore, as like in wild-type siblings, other *dscam* genes, *dscama* and *dscaml1*, are not expressed in *dscamb* mutant photoreceptors, suggesting no compensation for the loss of Dscamb by Dscam paralogs. Therefore, these two possibilities are unlikely. On the other hand, we found that Dscamb is dispensable for filopodium-mediated homotypic recognition and self-avoidance of blue cones. Thus, it is very likely that other self-avoidance molecules are involved in mosaic spacing of blue cones. Protocadherin (Pcdh) may be a promising candidate. Three *pcdh* genes, namely *pcdh8*, *pcdh10a*, and *pcdh10b*, are expressed in zebrafish photoreceptors at 48 hpf[49]. In addition, *pcdh11* is enriched in blue cones in zebrafish[50]. It will be interesting to examine whether these candidate genes are expressed in non-red cones, including blue cones, and if so, to generate their mutants for further analysis of cone mosaic phenotypes. Recently, it was reported that DSCAM functions as a general "nonstick" signal that masks a cell type-specific adhesion mechanism in soma spacing and dendrite arborization of mouse retinal ganglion cells[28,29]. If zebrafish Dscamb suppresses cell adhesion molecules whose expression is enriched only in red cones, few or no defects in mosaic spacing of UV and green cones in *dscamb* mutants can be explained. It is also possible that the stability of Dscamb protein is greater in red cones than in green and UV cones. In addition to homophilic interaction, DSCAM has several heterophilic interacting partners[51], for example, Deleted in Colorectal Cancer (DCC)[52] and UNC5[53] for axon guidance. There might be another cell-type-specific recognition coreceptor of Dscamb. In the future, it will be important to investigate expression profiles of cell adhesion molecules in each cone type and to generate a specific antibody against Dscamb protein for evaluation of these other possibilities.

The peripheral region of adult zebrafish retinas shows a lattice-like, regular cone mosaic pattern. In this study, we showed that Dscamb is required for the formation of this adult cone mosaic pattern. In the peripheral region of adult retinas, stem cells generate cones in a stepwise manner, which consists of three distinct zones in the CMZ: the progenitor proliferating zone, the pre-column zone, and the mature cone lattice zone, along the periphero-central axis[41,42]. We found that red cones extend filopodium-like neurites in the retinal CMZ to form the filopodium active zone, and that the regular red cone hexagonal pattern was affected in the pre-column zone in *dscamb* mutants, suggesting that as in embryonic retinas, Dscamb-mediated homotypic recognition regulates mosaic spacing of red cones in the CMZ of adult retinas. Müller cells promote the formation of the lattice-like cone mosaic pattern by mechanical regulation through adherens junctions between Müller cells and cones in the pre-column zone[41,42]. Indeed, N-cadherin signals representing adherens junctions between Müller cells and cones are markedly reduced in *dscamb* mutants, suggesting that Dscamb-mediated red cone spacing is required for Müller cell-mediated mechanical regulation to form the lattice-like cone mosaic. Thus, Dscamb-mediated homotypic cone spacing is the initial step of cone mosaic formation. In the future, it will be important to confirm whether apical filopodium-mediated recognition of the same cone type induces avoidance movements to achieve mosaic spacing in the retinal CMZ.

Lastly, our findings provide new insights for a mechanistic understanding of mosaic spacing of soma position in nervous system development, and open the way to investigate whether this filopodium-mediated and DSCAM-dependent cone mosaic formation is evolutionarily conserved among vertebrates.

Methods

Ethics statement

Zebrafish were maintained at 28.5 °C, on a 14-hour light/10-hour dark cycle, following standard procedures[54]. Embryos were collected and cultured in E3 embryo medium (5 mM NaCl, 0.17 mM KCl, 0.33 mM CaCl$_2$, 0.33 mM MgSO$_4$) supplemented with 0.0002 % methylene blue to prevent fungal growth. Experiments that investigated zebrafish embryonic cone mosaic patterns were conducted from the one-cell stage to 5 dpf prior to sexual differentiation. Thus, sexes of embryos could not be determined. Experiments that investigated zebrafish larval and adult cone mosaic patterns were carried out at 18 dpf, 3 wpf, 1.5 mpf, and 4 mpf. Both male and female fish were utilized to ensure consistency in the results. All zebrafish experiments were conducted in accordance with the OIST Animal Care and Use Program, adhering to the Guide for the Care and Use of Laboratory Animals by the National Research Council of the Nation Academies and were approved by the Association for Assessment and Accreditation of Laboratory Animal Care (AAALAC). The OIST Institutional Animal Care and Use Committee approved all experimental protocols (Protocol: ACUP-2023-016, ACUP -2023-017, ACUP -2023-018, ACUP -2023-019, ACUP -2023-020).

Zebrafish strains

Zebrafish (*Danio rerio*) were maintained using standard procedures[54]. Okinawa wild-type (oki) was used as a wild-type strain for mutagenesis in which *dscamb* mutant lines was generated. Two *dscamb* mutant alleles, *dscamb*[oki9] and *dscamb*[oki10] were used. Regarding zebrafish transgenic lines, *Tg[sws2:GFP]*[kjll32] and *Tg[thrb:tdTomato]*[q229] were used to visualize blue and red cones, respectively. *Tg[thrb:Gal4VP16]*[oki079] was created in our lab and used for expression of Gal4VP16 in red cones. *Tg[thrb:Gal4VP16]*[oki079] contains another DNA expression construct, *cmcl2:CFP*, which expresses CFP specifically in the heart for identifying transgenic embryos at 1 dpf without UAS-transgenic lines. *Tg[UAS:Dscamb-GFP]*[oki080] was created in our lab and used in combination with *Tg[hsp:gal4]*[kca455] to investigate subcellular localization of Dscamb protein in cones. *Tg[UAS:lifeact-GFP]*[rhi7] and *Tg[UAS:lifeact-mCherry]*[rhi4 40] were used in combination with *Tg[thrb:Gal4VP16]*[oki079] and *Tg[foxq2-2A-Gal4VP16]*[oki081], respectively, to visualize cone apical filopodia. *Tg[Ef1α:mCherry-CAAX]*[oki04956] was used to visualize plasma membrane of photoreceptors. *Tg[crx:mCFP]*[q209] was used to visualize all cones and their progenitors. *Tg[gnat2:ponli-GFP]*[oki082] was generated in our lab and used for visualization of Ponli localization in the pentameric cone unit. *Tg[gfap:GFP]*[mi2001] was used to visualize Müller cells[57]. Transgenic and mutant lines were combined with the zebrafish pigmentation mutants, *albino* (*alb*[b4])[58] and *roy orbison* (*roy*[a9])[59] to remove melanophores and iridophores, respectively for enhanced live imaging.

Preparation of DNA expression constructs, pTol2[thrb:Gal4VP16;cmcl2:CFP], pTol2[UAS:Dscamb-GFP], pTol2[UAS:mEGFP-Dscamb], and pTol2[gnat2:ponli-GFP]

Construct pTol2[thrb:Gal4VP16;cmcl2:CFP], used to establish the transgenic line Tg[thrb:Gal4VP16] [oki079], was prepared as follows. The construct pTol2[thrb:MCS], which was originally gifted from the Rachel Wong lab, has the thrb promoter with a multiple cloning site. A DNA fragment encoding Gal4VP16 was prepared by digestion of another DNA construct p[Nyx:Gal4VP16][60] with BamHI and ClaI, and subcloned into the pTol2[thrb:MCS] vector to prepare pTol2[thrb:Gal4VP16]. Then, pTol2[thrb:Gal4VP16] was used as a template to amplify a 3.8 kb DNA fragment encoding thrb:Gal4VP16 using Phusion High-Fidelity DNA polymerase (New England Biolabs (NEB), M0530S) with a pair of primers 5′- TTTTGGAGATCACTTGGGCCCAAGCTATCAACTTTGTATAGAA-3′ and 5′- TATCATGTCTGGATCATCATTACAGCTCATCCTTGTC CAGG-3′. After purification, the DNA fragment of thrb:Gal4VP16 was subcloned into the pTol2[MCS;cmcl2:CFP] vector digested with ApaI and ClaI, using NEBuilder® HiFi DNA Assembly Cloning Kit (NEB, E5520S).

Construct pTol2[UAS:Dscamb-GFP], used to establish the transgenic line Tg[UAS:Dscamb-GFP][oki080], was prepared as follows. A 6-kbp full-length dscamb cDNA fragment was amplified from zebrafish retinal cDNA pool with a pair of primers 5′- ACACGAATTCGCCACCATGTGGATATTGGCATTTCTCTTTCTCC-3′ and 5′- TCACACCTCCACCTCC CGATACAAGTGTGTAGGACTTTGCGTAGG-3, and subcloned into another expression construct pTol2[UAS:strip1-GFP][61] with NcoI and XhoI by replacing the strip1 cDNA fragment with the full-length dscamb cDNA fragment to prepare pTol2[UAS:Dscamb-GFP].

Construct pTol2[UAS:mEGFP-Dscamb] was made by fusing four fragments which were prepared either by digestion with a restriction enzyme or PCR. The UAS vector, with the signal peptide at the N-terminus, was from BglII-treated pTol2[UAS:Dscamb-GFP]. A DNA fragment encoding monomeric enhanced GFP (mEGFP) with a C-terminal linker was gifted from Dr. Bo Tang. Primer 5′-AGGACCTGCGTTCCAGCTTATATTTTGTCAATGCATC-3′ and 5′-TATCATGTCTGGATCATCATTCGAACGTGGTCCGTAGCTGTAGTCC-3′ were used to amplify the dscamb cDNA fragment without the signal peptide. A DNA fragment containing the last 180 bp of the dscamb coding sequence, SV40 poly A signals, and Tol2-R150 arm was collected from ApaI & KpnI-digested pTol2[UAS:nlsVenus-P2A-DscambICD], which we previously created to investigate the function of the intracellular domain of Dscamb.

Construct pTol2[gnat2:ponli-GFP], used to establish the transgenic line Tg[gnat2:ponli-GFP][oki082], was prepared as follows. Full-length cDNA of ponli, which is currently renamed pals1b in the ZFIN database, was amplified with PCR and tagged with GFP at the C-terminus. A DNA fragment encoding C-terminal GFP-tagged Ponli was subcloned into the Tol2 expression vector under the control of zebrafish cone-specific gnat2 promoter[62], to prepare pTol2[gnat2:ponli-GFP].

Generation of dscamb mutant strains

We generated zebrafish dscamb mutants, using CRISPR/Cas9. The gRNA sequence was designed to target exon 4 corresponding to the 2nd Ig-like domain, which is essential for homophilic interaction of DSCAM molecules (Supplementary Fig. 1), using an online tool https:// chopchop.cbu.uib.no/. To make gRNA, a set of primers, 5′- TAGGGACCGCATCATCACCACAGA-3′ and 5′-AAACTCTGTGGTGATGATGCG GTC-3′ were used for simple annealing for 1 min from 98 °C to room temperature. This annealed double-stranded DNA was subcloned into the pT7-gRNA plasmid vector[63] with restriction enzyme BsmBI. After this plasmid, pT7-dsacmb gRNA, was linearized with BamHI, this template DNA was used for synthesis of dscamb gRNA, using a MEGAshortscript™ T7 Transcription Kit (Thermo Fisher Scientific, AM1354). Next, wild-type fertilized eggs were injected with a 2-μL mixture of dscamb gRNA (200 ng/μL) and Cas9 nuclease (NEB,

M0386S) (500 ng/μl) and bred to the adult stage as the F0 generation. F0 adult fish were crossed with the wild-type strain to produce the F1 generation. To identify F1 fish carrying indel mutations in the dscamb gene, genomic DNA was extracted by fin clipping of each F1 fish and the genomic region covering gRNA target sequence was sequenced. Two frameshift mutants, dscamb[oki9] and dscamb[oki10], which carry 1-base- and 10-base deletions, respectively, were identified in the F1 generation and their mutant strains were established in the F2 generation. A pair of primers 5′-AAGATCCTCTCTGCCTTCAGC-3′ and 5′-TATTCGAGCCTGATAGGAGACC-3′ were used to amplify the genomic region covering these two deletion mutations. Restriction enzyme BsrGI was used for genotyping the dscamb[oki9] mutation. The genotype of the dscamb[oki10] mutation was identified based on the band size of the PCR product. To obtain chimeric wild-type retinas containing dscamb mutant cone photoreceptors, we injected dscamb gRNA/Cas9 complex into wild-type fertilized eggs, which carry the transgene Tg[thrb:tdTomato; sws2:GFP]. Injected F0 fish were bred at 1.5 mpf and used for confocal scanning of the retinal CMZ labeled with phalloidin.

To confirm that no off-target mutation occurred in other dscam genes, dscama and dscaml1, in two zebrafish dscamb mutant alleles, dscamb[oki9] and dscamb[oki10], we amplified a DNA fragment containing exon 4 of dscama gene using a primer pair, 5′-TCGATTTTTGT GTTTTTAGGGG-3′ and 5′-ACTTTTACCTGGCACAAAGAGC-3′, and a DNA fragment containing exon 4 of dscaml1 genes using a primer pair, 5′-GGGCATTTCCCCTCATCAGC-3′ and 5′-GTAGCATGCTCACCCAGAACAG-3′, for sequencing.

Generation of transgenic strains

For generation of three transgenic strains Tg[thrb:Gal4VP16][oki079], Tg[UAS:Dscamb-GFP][oki080], and Tg[gnat2:ponli-GFP][oki082], a mixture of Tol2 vector-based DNA constructs (20 ng/μL) and Tol2 transposase mRNA (20 ng/μL) were injected into wild-type fertilized eggs and bred to the adult stage as the F0 generation. F0 adult fish were crossed with the wild-type strain to produce the F1 generation. Founder fish were identified in F1 generation embryos and bred to establish the transgenic strains.

For generation of a knock-in transgenic strain, Tg[foxq2-2A-Gal4VP16; UAS:EGFP][oki081], DNA fragment encoding Gal4VP16 was amplified from the p[Nyx:Gal4VP16] plasmid[60] by PCR using a pair of primers 5′- CAAGCAGGAGACGTGGAAGAAAACCCCGGTCCTATGAAG CTACTGTCTTCTATCGAAC-3′ and 5′-CTTGTACAGAGACGACTACATATCCAGAGCGCCGTAG-3′. The PCR product of Gal4VP16 and the pGTag-2A-eGFP-B-actin plasmid (addgene, 117814)[64] was digested with BsmBI and BsrGI restriction enzymes and ligated to make the pGTag-P2A-Gal4VP16-B-actin construct. Finally, the DNA fragment encoding the P2A-Gal4VP16 was amplified from the pGTag-P2A-Gal4VP16-B-actin construct by PCR, using primers 5′- GGTCATTTCTGGGCAATTCCAGGATCCGGAGCCACGAAC-3′ and 5′- TTGAAAGTTGGCCGGGTCTACATATCCAGAGCGCCGTAG-3′. Next, the genomic fragment containing the zebrafish foxq2 transcription unit, which consists of 2 exons and 1 intron, was amplified from zebrafish genomic DNA using a set of primers 5′- GCAGGCTGGAGACGTGGAGGAGAACCCTGGTCCTATGAACT TGGATCCAAAAACTGAACTTTC-3′ and 5′- TGCATCGATTTATATGAG TCCATGAAGGGCCGG-3′, and then was subcloned into a pCR II vector (Thermo Fisher Scientific, 450640). This zebrafish foxq2 transcription unit plasmid was linearized with CRISPR/Cas9 complex with foxq2 gRNA (5′-TCATTTCTGGGCAATTCACCCGG-3′), which was designed to target exon 2 of the foxq2 gene from a previous study[65]. This linearized zebrafish foxq2 transcription unit plasmid and the P2A-Gal4VP16 DNA fragment were integrated through NEBuilder® HiFi DNA assembly Cloning Kit (NEB, E5520S) to form the donor plasmid, which was subsequently digested with HindIII and ClaI to produce the donor dsDNA flanked by two homology arms with lengths of 1.1 kb and 250b, respectively. Inspired by another study that modified the 5′ end of donor DNA to increase the knock-in efficiency[66], we treated the donor

dsDNA with Alkaline Phosphatase (CIAP) (TaKaRa, 2250 A) to prevent potential concatenation of DNA fragments during genome integration. The donor dsDNA, *foxq2* gRNA, and Cas9 nuclease (NEB, M0386S) were assembled in Cas9 working buffer (20 mM HEPES; 150 mM KCl, pH 7.5) with final concentrations of 20 ng/μL, 50 ng/μL, and 250 ng/μL, respectively. The mixture was injected into *Tg[UAS:EGFP]* fertilized eggs and around 30 embryos expressing EGFP in the eye were selected for breeding. Among them, two F0 founder fish were identified to produce knock-in transgenic progeny F1. Using the same approach, we attempted to make 2A-Gal4VP16-reporter knock-in fish for the *dscamb* gene by targeting exon 4 (gRNA: 5'-ATATTTATCGCTGTACCACGCGG-3') and exon 33 (gRNA: 5'-CTGTACCGCCTCTCTGCTGGGGG-3'). However, due to the low integration efficiency, we did not recover these knock-in lines in the F1 generation, although we generated photoreceptors, in which a DNA fragment encoding 2A-Gal4VP16 was inserted in frame into exon 4 and exon 33 in F0 injected embryos, in a mosaic manner.

Retina flat mounting and immunolabeling

Fish were dark-adapted overnight in a small tank wrapped with aluminum foil. The next morning, 0.02% Ethyl 3-Aminobenzoate Methanesulfonate (Tricaine, MS-222) (Nacalai tesque, 1485-82) was added to the tank to fully anesthetize fish. Under dim light, fish were decapitated, and the eyes were quickly removed and placed in a petri dish with Leibovitz's L-15 medium (L15 medium) (Gibco, 41300039). A microscalpel and precision tweezers were used to remove the sclera, retinal pigment epithelium, and lens. After the retina was exposed, several cuts were made to flatten the retina, which was then fixed in 4% PFA (dissolved in PO_4 buffer (0.1 M, pH7.3) with 5% sucrose) overnight at 4 °C. PFA-fixed samples were washed with PO_4 buffer for 3 x 10 min and used for confocal scanning. Hoechst 33342 (Wako, 346-07951) was used at 1 ng/mL for counter-staining of nuclei.

We performed immuno-labeling for 4 mpf flat-mounted retinas carrying transgenes *Tg[thrb:tdTomato; sws2:GFP]* with anti-N-cadherin antibody (rabbit polyclonal, Abcam, ab211126, 1:200) or anti-Crb2b-lf antibodies (rat polyclonal, 1:50), as described previously[67]. Embryonic eyes at 5 dpf were isolated and stained with zpr1 antibody (mouse monoclonal, Zebrafish International Resource Center (ZIRC), 1:200). To counterstain GFP and tdTomato, we used anti-rabbit Alexa 633 antibody (Thermo Fisher Scientific, A21071, 1:500) and anti-rat Alexa 633 antibody (Thermo Fisher Scientific, A21094, 1:500) to detect anti-N-cadherin and anti-Crb2b signals, respectively, and anti-mouse Alexa 647 antibody (Thermo Fisher Scientific, A21236, 1:500) to detect zpr1 signals. After staining, samples were washed again with PO_4 buffer for 3 x 10 min. After the final wash, PO_4 buffer was replaced with RapiClear1.49 (SunJin Lab, RC149001) for more than 1 h at room temperature to make the retina more transparent. The retina was placed in the center of a spacer on a glass slide, and mounted with RapiClear1.49 as the photoreceptor side of the retina was oriented close to the cover slide.

In situ hybridization

For the preparation of a *dscamb* RNA probe, a template plasmid of zebrafish *dscamb* cDNA was constructed as follows. First, the full-length *dscamb* cDNA was amplified from a zebrafish retinal cDNA pool with PCR using a pair of primers: 5'-GCTTGGGGATTGAACGCAGC-3' and 5'-CGTGGTCCGTAGCTGTAGTCC-3', and subcloned into the pCRII vector (Thermo Fisher Scientific, 450640) using TA Cloning Kit (Thermo Fisher Scientific, K207020). This full-length *dscamb* cDNA plasmid was digested with SpeI to produce a DNA fragment containing the pCRII vector and the 0.9-kb intracellular domain of *dscamb* cDNA. This short linear DNA fragment was self-ligated to prepare a new pCRII plasmid carrying the 0.9 kb *dscamb* intracellular domain, which was used for synthesis of sense and anti-sense RNA probes. For preparation

of a *thrb* RNA probe, a 1-kb *thrb* cDNA fragment with the T7 promoter at one end was amplified with PCR using a pair of primers: 5'-TAATACGACTCACTATAGGGAGACAACACCCAAACCCCC-3' and 5'-CATGGTGTAAGTGGCGGATATG-3'. This purified PCR product was directly used as a template for RNA probe synthesis.

To amplify cDNA fragments of *dscama* and *dscaml1* for in situ hybridization, primers modified from a previous study[31] were used. 5'-GCTCTGAGTCCAGCTGAGAAA-3', and 5'-TAATACGACTCACTATAGGGAGAGGATCCCTGGGACGTTGTAG-3' were designed to clone *dscama* cDNA fragment, whereas 5'-GGGCTCATCCAGCTGACAG-3', and 5'-TAATACGACTCACTATAGGGAGATCTCCCCATTCTCCATCGGG-3' were used for *dscaml1*. A T7 promoter sequence was added to the primer pairs and the PCR products were purified for RNA probe synthesis.

Embryos or retinas were fixed with fresh 4% PFA overnight at 4 °C. After washing with PBS 3 x 10 min, PFA-fixed samples were dehydrated with 100% methanol and then stored at -30 °C for future use. *dscamb* and *thrb* RNA probes were synthesized using a DIG RNA labeling Mix (Merck, 11277073910) and a Fluorescein RNA Labeling Mix (Merck, 11685619910), respectively. Following a published protocol[68], samples stored in methanol were rehydrated in PBS, hybridized with RNA probes at 65°C overnight, and washed with 0.5xSSC/0.1% Tween20 at 65 °C for 3 x 30 min. Next, samples were treated with anti-DIG alkaline phosphatase (AP)-conjugated antibody (Merck, 11093274910, 1:1000) for 1 h at room temperature or overnight at 4 °C. Then, they were washed with maleic acid buffer/0.1% Tween20 for 4 x 15 min and incubated with Tris-HCl buffer (pH9.5) containing AP substrate BM purple (Merck, 11442074001) for color development of mRNA signals. After samples were transferred to 70% glycerol, whole-mount images were captured with a dissecting microscope (ZEISS SteREO Discovery.V12). To show cross-sectional views of 1.5-mpf retinas, we dissected retinal specimens into small slices for imaging.

For two-color fluorescence in situ hybridization, either *dscamb* or *thrb* RNA probe was applied to tissue samples at a final concentration 0.5 ng/μL. After washing with 0.5xSSC/0.1% Tween 20, samples were soaked in 2% blocking reagent (Merck, 11096176001) overnight at 4 °C or 1 h at room temperature. Then, samples were treated with anti-Fluorescein POD-conjugated antibody (Merck, 11426346910) (1:500 in 2% block solution) for 1.5 h at room temperature. Stringent washing was done before applying TSA Plus Fluorescein (AKOYA, NEL741001KT) (1:50 in amplification buffer) for 1 h at room temperature. Samples were then dehydrated with methanol gradients and were immersed in 1% H_2O_2 in methanol for 30 min. Following rehydration and blocking, anti-DIG-POD-conjugated antibody (Merck, 11207733910) (1:1000 in 2% block solution) was applied for 1.5 h at room temperature. After stringent washing, samples were treated with TSA Plus Cyanine 5 (AKOYA, NEL745001KT) (1:50 in amplification buffer) for 1 h at room temperature. Eventually, samples were subjected to glycerol gradients (30%, 50%, 70% in PBS) and were placed in a glass-bottomed petri dish for imaging using an SP8 confocal microscope (Leica).

Transplantation

Cell transplantation was carried out at the blastula stage as preciously described[69]. Cascade Blue dextran (Thermo Fisher Scientific, D1976) (1% in 200 mM KCl) was injected into fertilized eggs to label donor cells. We transplanted *dscamb* mutant cells into wild-type host embryos and vice versa. Both host and donor embryos carry *Tg[thrb:tdTomato]* to visualize red cones. Either the donor or host embryos or both carried *Tg[thrbGal4VP16; UAS:lifeact-GFP]* to visualize apical filopodia. Using 1-h time-lapse imaging data of 52-hpf transplanted retinas, we analyzed filopodium behavioral dynamics during the interaction between *dscamb* mutant red cones and wild-type red cones.

Time-lapse live imaging of apical filopodium extension behaviors of cones

To inhibit melanophore pigmentation, 1-phenyl-2-thiourea (PTU) (Nacalai tesque, 27429-22), was added at 0.003% to E3 embryonic medium from 7 hpf. At 52 hpf, we selected *Tg[thrb:Gal4VP16; UAS:lifeact-GFP; thrb:tdTomato]* transgenic embryos, which normally show high GFP expression in the eye, but only small, dot-like tdTomato signals in the ventral retina. These transgenic embryos were anesthetized with 0.02% tricaine, washed briefly with L15 medium (Gibco, 41300039) twice, and transferred to a small petri dish with a glass bottom for imaging. We dissected and removed the eyes with precision tweezers by excising surrounding tissues. Remaining embryonic bodies were used for genotyping. Eyes were oriented with the lens side up. By gently touching the cornea, the eyes readily attached to a clean glass bottom. The dish was then mounted on a Leica SP8 confocal microscope using a 40X water-immersion objective lens. Higher scanning speed (~ 20 s per frame) and continuous mode (no interval time) were adopted to capture active movement of filopodia at the OLM. To avoid potential damage to cultured retinas, we kept the energy of the lasers at a low level and confirmed that within the first ~5 h of continuous scanning, cells remained active. No incubator with carbon dioxide supply was used. Room temperature was set to 23 °C. Immersion oil with a refractive index=1.3 (similar to water) was applied.

Regarding sampling of red cone filopodia (Fig. 3c and Supplementary Fig. 4) for statistical evaluation (Fig. 3e–h), three representative red cones were used for sampling 13 filopodia for wild-type sibling embryos and 14 filopodia for *dscamb* mutant embryos. Each of three representative red cones was selected from different embryos according to the following procedure. First, red cones had filopodia that showed active dynamics of extension and retraction. Second, red cones were surrounded by at least 4 red cones without or with barely detectable Lifeact-GFP expression. Finally, only a red cone that had the highest number of interacting red cones was selected from red cones that satisfied the first and second criteria. After the selection of representative red cones, we selected 4-5 filopodia for measurement of the distance from tips to interacting red cone borderlines. If a red cone had multiple filopodia interacting with the same neighboring red cone, we selected only one filopodium, in which the filopodial tip didn't contact the neighboring red cone at the beginning and had a clear extension/retraction cycle in the time-lapse movie. Movies were processed using Imaris ver.9.5.1 (Bitplane). Two movies for wild-type/heterozygous and *dscamb* mutant retinas were combined using an open source video editor, Shotcut ver. 24.02.29 (Meltytech, LLC).

Computer simulation

For the simulation, we first created a random red cone mosaic. Each red cone had 12 filopodia evenly distributed in 12 directions. Initial filopodia were also randomly set as retracting or extending filopodia with random length between the maximum (l_{max}) and the minimum length ($l_{min} = 0$). Over Δt, new values for positions of red cones and their tips were calculated with the following equations. Specifically, for a certain red cone, after Δt (or the next step in simulation),

$$\Delta \mathbf{R} = k \sum_i \mathbf{F}_i \qquad (1)$$

$$|\mathbf{F}| \propto l \qquad (2)$$

the centroid would move $\Delta \mathbf{R}$, which was decided by the net force generated by all retracting filopodia multiplied by a coefficient k (1). The pulling force $\mathbf{F}$ of a retracting filopodium was proportional to its length l (2). $f_{ER} = 1$ ($f_{ER} = -1$) indicates that a filopodium was extending (retracting).

If the length of a retracting filopodium was negative in the next step, it began to extend (3).

$$\text{If } l < 0; \text{ then } f_{ER} = 1 \qquad (3)$$

If an extending filopodium reached the maximum length, it began to retract in the next step (4).

$$\text{If } l > l_{max}; \text{ then } f_{ER} = -1 \qquad (4)$$

Extending and retracting speeds for filopodia were the same.

In the wild type, if the coordinates of a filopodium tip $\mathbf{f}_{tip}$ were inside another red cone ($\mathbf{R}_{other}$ represented the centroid of another red cone), meaning the tip contacted another red cone with radius r, it began to retract in the next step (5). In the mutant, this homotypic recognition was masked.

$$|\mathbf{f}_{tip} - \mathbf{R}_{other}| < r; \text{ then } f_{ER} = -1 \qquad (5)$$

For the simulation incorporating sticky filopodial tips (Supplementary Fig. 6), a parameter called the slowing down coefficient (slc) was introduced to control the retracting speed of filopodia if their tips were inside other red cones. After this condition was applied, filopodia retracted at a speed *v* (6). Here, v0 represented the default retracting speed. Once the tips detached from other red cones, the retracting speed returned to v0.

$$v = v0 * slc \, (0 < slc < 1) \qquad (6)$$

The simulation was performed using Python 3.8.5 (Phyton Software Foundation). At each step, a new plot was created and saved. ImageJ (NIH) was used to sort and convert all plots into a dynamic movie. The original script is available in an open-source repository, Code Ocean. The code can be found at https://doi.org/10.24433/CO.2519175.v1.

Quantification and statistical analysis

We measured the length of the borderline between cones using confocal images at the OLM level, and calculated the percentage of homotypic and heterotypic contacts for each cone-type (Fig. 1d). To quantify the regularity of each cone type spacing (Fig. 1e, h) the conventional nearest neighbor distance (NND)-derived regularity index (RI) was used[33]. Using ImageJ (NIH), centroids of cones were identified and exported to calculate the regularity index with the equation RI = NND/standard deviation (SD). Marginal cones were excluded from the calculation. To quantify cone density (Fig. 1f, i), cones were not included if they touched the image margin. In ex vivo time-lapse live imaging (Fig. 3d–h), red cones that failed to recognize other neighboring red cones were defined only if one of their filopodia invaded another red cone territory for >2 μm, which is nearly half the size of the apical domain of red cones, within the first 1 h of imaging. The percentage of the number of invading red cones relative to the number of all Lifeact-GFP positive red cones in the imaging frame (marginal cones were excluded) was calculated (Fig. 3d). For each filopodium, the distance from the tip to neighboring red cones was measured for each video frame and exported for a trajectory plot in GraphPad Prism 9.1.0 (GraphPad Software) (Fig. 3c, Supplementary Fig. 4a, b). Comparison plots were generated in GraphPad Prism 9.1.0 using non-paired t-tests (Fig. 3e, h, j). For the fraction of red cone precursors/their progeny red cones, which were contacted by other red cones or isolated from other red cones, a histogram was generated in GraphPad Prism 9.1.0. using chi-squared test (Fig. 5b). For in vivo temporal profiles and simulation of cone spacing patterns (Fig. 5c, g), red cones were tracked using the TrackMate plugin in Fiji/ImageJ Ver.2.14.0/1.54 f (NIH).

Position values of cells in each frame were exported for regularity index calculation. Means of the regularity index of every 20 frames were plotted (Fig. 5d, h). Paired t-tests were performed for both time-lapse imaging (Fig. 5e) and simulation (Fig. 5i). Statistical analysis was conducted using GraphPad Prism 9.1.0. Data are represented as means ± SD. Details of statistical tests and number of samples used are in figures and figure legends.

Reporting summary

Further information on research design is available in the Nature Portfolio Reporting Summary linked to this article.

Data availability

All the data for the analyses presented in this study are provided in the Source Data file. Source data are provided with this paper.

Code availability

The original script for computer simulation is available in an open-source repository, Code Ocean. The code can be found in https://doi.org/10.24433/CO.2519175.v1.

References

1. Viets, K., Eldred, K. & Johnston, R. J. Jr. Mechanisms of photoreceptor patterning in vertebrates and invertebrates. *Trends Genet* **32**, 638–659 (2016).
2. Nawrocki, L., BreMiller, R., Streisinger, G. & Kaplan, M. Larval and adult visual pigments of the zebrafish, Brachydanio rerio. *Vis. Res* **25**, 1569–1576 (1985).
3. Branchek, T. & Bremiller, R. The development of photoreceptors in the zebrafish, Brachydanio rerio. I. Structure. *J. Comp. Neurol.* **224**, 107–115 (1984).
4. Larison, K. D. & Bremiller, R. Early onset of phenotype and cell patterning in the embryonic zebrafish retina. *Development* **109**, 567–576 (1990).
5. Zou, J., Wang, X. & Wei, X. Crb apical polarity proteins maintain zebrafish retinal cone mosaics via intercellular binding of their extracellular domains. *Dev. Cell* **22**, 1261–1274 (2012).
6. Zou, J., Yang, X. & Wei, X. Restricted localization of ponli, a novel zebrafish MAGUK-family protein, to the inner segment interface areas between green, red, and blue cones. *Invest Ophthalmol. Vis. Sci.* **51**, 1738–1746 (2010).
7. Allison, W. T. et al. Ontogeny of cone photoreceptor mosaics in zebrafish. *J. Comp. Neurol.* **518**, 4182–4195 (2010).
8. Boije, H., Rulands, S., Dudczig, S., Simons, B. D. & Harris, W. A. The independent probabilistic firing of transcription factors: a paradigm for clonal variability in the zebrafish retina. *Dev. Cell* **34**, 532–543 (2015).
9. Suzuki, S. C. et al. Cone photoreceptor types in zebrafish are generated by symmetric terminal divisions of dedicated precursors. *Proc. Natl Acad. Sci.* **110**, 15109–15114 (2013).
10. Ogawa, Y., Shiraki, T., Fukada, Y. & Kojima, D. Foxq2 determines blue cone identity in zebrafish. *Sci. Adv.* **7**, eabi9784 (2021).
11. Alvarez-Delfin, K. et al. Tbx2b is required for ultraviolet photoreceptor cell specification during zebrafish retinal development. *Proc. Natl Acad. Sci. USA* **106**, 2023–2028 (2009).
12. Ogawa, Y. et al. Six6 and Six7 coordinately regulate expression of middle-wavelength opsins in zebrafish. *Proc. Natl Acad. Sci. USA* **116**, 4651–4660 (2019).
13. Raymond, P. A. et al. Patterning the cone mosaic array in zebrafish retina requires specification of ultraviolet-sensitive cones. *PLoS One* **9**, e85325 (2014).
14. Hao, Q. et al. Crumbs proteins stabilize the cone mosaics of photoreceptors and improve vision in zebrafish. *J. Genet. Genomic.* https://doi.org/10.1016/j.jgg.2020.12.002 (2021).
15. Dong, H., Li, J., Wu, Q. & Jin, Y. Confluence and convergence of Dscam and Pcdh cell-recognition codes. *Trends Biochem Sci.* **48**, 1044–1057 (2023).
16. Millard, S. S., Flanagan, J. J., Pappu, K. S., Wu, W. & Zipursky, S. L. Dscam2 mediates axonal tiling in the Drosophila visual system. *Nature* **447**, 720–724 (2007).
17. Fuerst, P. G., Koizumi, A., Masland, R. H. & Burgess, R. W. Neurite arborization and mosaic spacing in the mouse retina require DSCAM. *Nature* **451**, 470–474 (2008).
18. Schmucker, D. et al. Drosophila Dscam is an axon guidance receptor exhibiting extraordinary molecular diversity. *Cell* **101**, 671–684 (2000).
19. Wojtowicz, W. M., Flanagan, J. J., Millard, S. S., Zipursky, S. L. & Clemens, J. C. Alternative splicing of Drosophila Dscam generates axon guidance receptors that exhibit isoform-specific homophilic binding. *Cell* **118**, 619–633 (2004).
20. Neves, G., Zucker, J., Daly, M. & Chess, A. Stochastic yet biased expression of multiple Dscam splice variants by individual cells. *Nat. Genet* **36**, 240–246 (2004).
21. Dong, H. et al. Hidden RNA pairings counteract the "first-come, first-served" splicing principle to drive stochastic choice in Dscam1 splice variants. *Sci. Adv.* **8**, eabm1763 (2022).
22. Zhan, X. L. et al. Analysis of Dscam diversity in regulating axon guidance in Drosophila mushroom bodies. *Neuron* **43**, 673–686 (2004).
23. Zhu, H. et al. Dendritic patterning by Dscam and synaptic partner matching in the Drosophila antennal lobe. *Nat. Neurosci.* **9**, 349–355 (2006).
24. Hummel, T. et al. Axonal targeting of olfactory receptor neurons in Drosophila is controlled by Dscam. *Neuron* **37**, 221–231 (2003).
25. Wang, J., Zugates, C. T., Liang, I. H., Lee, C. H. & Lee, T. Drosophila Dscam is required for divergent segregation of sister branches and suppresses ectopic bifurcation of axons. *Neuron* **33**, 559–571 (2002).
26. Hattori, D. et al. Dscam diversity is essential for neuronal wiring and self-recognition. *Nature* **449**, 223–227 (2007).
27. Liu, C. et al. Dscam1 establishes the columnar units through lineage-dependent repulsion between sister neurons in the fly brain. *Nat. Commun.* **11**, 4067 (2020).
28. Fuerst, P. G. et al. DSCAM and DSCAML1 function in self-avoidance in multiple cell types in the developing mouse retina. *Neuron* **64**, 484–497 (2009).
29. Garrett, A. M., Khalil, A., Walton, D. O. & Burgess, R. W. DSCAM promotes self-avoidance in the developing mouse retina by masking the functions of cadherin superfamily members. *Proc. Natl Acad. Sci. USA* **115**, E10216–E10224 (2018).
30. Arimura, N. et al. DSCAM regulates delamination of neurons in the developing midbrain. *Sci. Adv.* **6** https://doi.org/10.1126/sciadv.aba1693 (2020).
31. Galicia, C. A., Sukeena, J. M., Stenkamp, D. L. & Fuerst, P. G. Expression patterns of dscam and sdk gene paralogs in developing zebrafish retina. *Mol. Vis.* **24**, 443–458 (2018).
32. Takechi, M., Seno, S. & Kawamura, S. Identification of cis-acting elements repressing blue opsin expression in zebrafish UV cones and pineal cells. *J. Biol. Chem.* **283**, 31625–31632 (2008).
33. Keeley, P. W., Eglen, S. J. & Reese, B. E. From random to regular: Variation in the patterning of retinal mosaics. *J. Comp. Neurol.* **528**, 2135–2160 (2020).
34. Raymond, P. A. & Barthel, L. K. A moving wave patterns the cone photoreceptor mosaic array in the zebrafish retina. *Int J. Dev. Biol.* **48**, 935–945 (2004).
35. Raymond, P. A., Barthel, L. K. & Curran, G. A. Developmental patterning of rod and cone photoreceptors in embryonic zebrafish. *J. Comp. Neurol.* **359**, 537–550 (1995).

36. Julien, D. P. et al. Zebrafish expression reporters and mutants reveal that the IgSF cell adhesion molecule Dscamb is required for feeding and survival. *J. Neurogenet.* **32**, 336–352 (2018).

37. Yamagata, M. & Sanes, J. R. Synaptic localization and function of Sidekick recognition molecules require MAGI scaffolding proteins. *J. Neurosci.* **30**, 3579–3588 (2010).

38. Garrett, A. M., Tadenev, A. L., Hammond, Y. T., Fuerst, P. G. & Burgess, R. W. Replacing the PDZ-interacting C-termini of DSCAM and DSCAML1 with epitope tags causes different phenotypic severity in different cell populations. *Elife* **5** https://doi.org/10.7554/eLife.16144 (2016).

39. Aparicio, G., Rodao, M., Badano, J. L. & Zolessi, F. R. Photoreceptor progenitor dynamics in the zebrafish embryo retina and its modulation by primary cilia and N-cadherin. *Int J. Dev. Biol.* **65**, 439–455 (2021).

40. Mizoguchi, T., Kawakami, K. & Itoh, M. Zebrafish lines expressing UAS-driven red probes for monitoring cytoskeletal dynamics. *Genesis* **54**, 483–489 (2016).

41. Nagashima, M., Hadidjojo, J., Barthel, L. K., Lubensky, D. K. & Raymond, P. A. Anisotropic Muller glial scaffolding supports a multiplex lattice mosaic of photoreceptors in zebrafish retina. *Neural Dev.* **12**, 20 (2017).

42. Salbreux, G., Barthel, L. K., Raymond, P. A. & Lubensky, D. K. Coupling mechanical deformations and planar cell polarity to create regular patterns in the zebrafish retina. *PLoS Comput Biol.* **8**, e1002618 (2012).

43. Lyall, A. H. Cone arrangements in teleost retinae. *Quart. J. Microsc Sci.* **98**, 189–201 (1957).

44. Engström, K. Cone types and cone arrangements in teleost retinae1. *Acta Zoologica* **44**, 179–243 (1963).

45. Sharkova, M., Aparicio, G., Mouzaaber, C., Zolessi, F. R. & Hocking, J. C. Photoreceptor calyceal processes accompany the developing outer segment, adopting a stable length despite a dynamic core. *J. Cell Sci.* **137** https://doi.org/10.1242/jcs.261721 (2024).

46. Kozlowski, C., Hadyniak, S. E. & Kay, J. N. Retinal neurons establish mosaic patterning by excluding homotypic somata from their dendritic territories. *Cell Rep.* **43**, 114615 (2024).

47. Kay, J. N., Chu, M. W. & Sanes, J. R. MEGF10 and MEGF11 mediate homotypic interactions required for mosaic spacing of retinal neurons. *Nature* **483**, 465–469 (2012).

48. Tohya, S., Mochizuki, A. & Iwasa, Y. Difference in the retinal cone mosaic pattern between zebrafish and medaka: cell-rearrangement model. *J. Theor. Biol.* **221**, 289–300 (2003).

49. Xu, B. et al. Unifying developmental programs for embryonic and postembryonic neurogenesis in the zebrafish retina. *Development* **147,** https://doi.org/10.1242/dev.185660 (2020).

50. Ogawa, Y. & Corbo, J. C. Partitioning of gene expression among zebrafish photoreceptor subtypes. *Sci. Rep.* **11**, 17340 (2021).

51. Hizawa, K., Sasaki, T. & Arimura, N. A comparative overview of DSCAM and its multifunctional roles in Drosophila and vertebrates. *Neurosci. Res* **202**, 1–7 (2024).

52. Ly, A. et al. DSCAM is a netrin receptor that collaborates with DCC in mediating turning responses to netrin-1. *Cell* **133**, 1241–1254 (2008).

53. Purohit, A. A. et al. Down syndrome cell adhesion molecule (DSCAM) associates with uncoordinated-5C (UNC5C) in netrin-1-mediated growth cone collapse. *J. Biol. Chem.* **287**, 27126–27138 (2012).

54. Westerfield, M. *The zebrafish book. A guide for the laboratory use of zebrafish (Danio rerio).* 4th edn, (Univ. of Oregon Press, Eugene., 2000).

55. Scheer, N., Riedl, I., Warren, J. T., Kuwada, J. Y. & Campos-Ortega, J. A. A quantitative analysis of the kinetics of Gal4 activator and effector gene expression in the zebrafish. *Mech. Dev.* **112**, 9–14 (2002).

56. Mochizuki, T., Luo, Y. J., Tsai, H. F., Hagiwara, A. & Masai, I. Cell division and cadherin-mediated adhesion regulate lens epithelial cell movement in zebrafish. *Development* **144**, 708–719 (2017).

57. Bernardos, R. L. & Raymond, P. A. GFAP transgenic zebrafish. *Gene Expr. Patterns* **6**, 1007–1013 (2006).

58. Haffter, P. et al. Mutations affecting pigmentation and shape of the adult zebrafish. *Dev. Genes Evol.* **206**, 260–276 (1996).

59. D'Agati, G. et al. A defect in the mitochondrial protein Mpv17 underlies the transparent casper zebrafish. *Dev. Biol.* **430**, 11–17 (2017).

60. Schroeter, E. H., Wong, R. O. & Gregg, R. G. In vivo development of retinal ON-bipolar cell axonal terminals visualized in nyx::MYFP transgenic zebrafish. *Vis. Neurosci.* **23**, 833–843 (2006).

61. Ahmed, M., Kojima, Y. & Masai, I. Strip1 regulates retinal ganglion cell survival by suppressing Jun-mediated apoptosis to promote retinal neural circuit formation. *Elife* **11** https://doi.org/10.7554/eLife.74650 (2022).

62. Kennedy, B. N. et al. Identification of a zebrafish cone photoreceptor-specific promoter and genetic rescue of achromatopsia in the nof mutant. *Invest Ophthalmol. Vis. Sci.* **48**, 522–529 (2007).

63. Jao, L. E., Wente, S. R. & Chen, W. Efficient multiplex biallelic zebrafish genome editing using a CRISPR nuclease system. *Proc. Natl Acad. Sci. USA* **110**, 13904–13909 (2013).

64. Wierson, W. A. et al. Efficient targeted integration directed by short homology in zebrafish and mammalian cells. *Elife* **9** https://doi.org/10.7554/eLife.53968 (2020).

65. Angueyra, J. M. et al. Transcription factors underlying photoreceptor diversity. *Elife* **12** https://doi.org/10.7554/eLife.81579 (2023).

66. Mi, J. & Andersson, O. Efficient knock-in method enabling lineage tracing in zebrafish. *Life Sci Alliance* **6** https://doi.org/10.26508/lsa.202301944 (2023).

67. Kujawski, S. et al. Loss of Crb2b-lf leads to anterior segment defects in old zebrafish. *Biol Open* **9** https://doi.org/10.1242/bio.047555 (2020).

68. Thisse, C. & Thisse, B. High-resolution in situ hybridization to whole-mount zebrafish embryos. *Nat. Protoc.* **3**, 59–69 (2008).

69. Kemp, H. A., Carmany-Rampey, A. & Moens, C. Generating chimeric zebrafish embryos by transplantation. *J Vis Exp* https://doi.org/10.3791/1394 (2009).

Acknowledgements

Author contributions

D.H. initiated the project in the group of I.M. D.H. designed experiments, analyzed the data and developed the project through the discussion with I.M. D.H. performed all the experiments. D.H. wrote the first draft of the manuscript with substantial input from I.M. D.H., and I.M. edited the subsequent draft of the manuscript. I.M. supervised and acquired funding for the project.

Competing interests

The authors declare no competing interests.

Additional information